NASA TECHNICAL NOTE

NASA TN D-3390

NASA TN D-3390

AERODYNAMICS OF AIRFRAME-ENGINE INTEGRATION OF SUPERSONIC AIRCRAFT

by Mark R. Nichols

Langley Research Center
Langley Station, Hampton, Va.

NATIONAL AERONAUTICS AND SPACE ADMINISTRATION • WASHINGTON, D. C. • AUGUST 1966

NASA TN D-3390

AERODYNAMICS OF AIRFRAME-ENGINE INTEGRATION OF SUPERSONIC AIRCRAFT

By Mark R. Nichols

Langley Research Center
Langley Station, Hampton, Va.

NATIONAL AERONAUTICS AND SPACE ADMINISTRATION

For sale by the Clearinghouse for Federal Scientific and Technical Information
Springfield, Virginia 22151 – Price $2.00

AERODYNAMICS OF AIRFRAME-ENGINE INTEGRATION OF SUPERSONIC AIRCRAFT*

By Mark R. Nichols
Langley Research Center

SUMMARY

Some major aerodynamic problems involved in the design of the propulsion-system installations of advanced supersonic aircraft are reviewed from the airframe viewpoint. Consideration is given to environmental factors such as flow fields, the airframe boundary layer, airframe-inlet and inlet-inlet shock interference, and jet-airframe interference. New aerodynamic tools available to the designer are discussed and are used along with experimental data to analyze the drag minimization problem. Finally, detailed attention is given to the problem of optimizing the propulsion system itself from the standpoint of inlet and nozzle selection, flow distortion effects, handling of the various secondary airflows, and afterbody drag.

INTRODUCTION

Manned aircraft have now been flying supersonically for nearly 19 years. Most of the supersonic flight time to date has been accumulated in brief dashes by aircraft optimized primarily for subsonic operation. The recent flights of the XB-70A and the A-11/SR-71, however, mark the advent of an entirely new class of vehicle optimized primarily for supersonic operation.

The propulsion systems of the new supersonic aircraft differ markedly from those of previous aircraft as a consequence of the much higher level of propulsion-system efficiency required. The designer cannot afford to let this efficiency slip more than several percent below the theoretical optimum, even at the expense of increased complexity and weight. At the same time, interactions between the airframe and the engine have become of even greater significance than previously. It is no longer possible to think in terms of optimizing a propulsion package and then attaching it to a separately optimized airframe. The two parts must be designed together and fully integrated in all respects. The purpose of this paper is to review major aerodynamic aspects of this integration problem.

---

*This material was originally presented at the 27th Meeting of the AGARD Propulsion and Energetics Panel, Paris, France, April 4, 1966.

SYMBOLS

A	area
A_{2b}	cross-sectional area of two nacelle bases
A_{lip}	area at cowl lip
A_{2N}	cross-sectional area of two nacelles
A_{4N}	cross-sectional area of four nacelles
A_{xs}	area of excess flow
$A_{\beta,proj}$	projected boattail area
b	wing span
C_D	drag coefficient
$C_{D,b}$	base drag coefficient
$C_{D,W}$	wave drag coefficient
$C_{D,\beta}$	boattail drag coefficient
C_L	lift coefficient
C_N	normal-force coefficient
C_p	pressure coefficient, $\frac{p - p_\infty}{q_\infty}$
$C_{p,b}$	base pressure coefficient
$C_{p,R}$	resultant load coefficient (top-surface C_p minus bottom-surface C_p)
d	diameter
D	drag

D_{byp}	bypass drag
$D_{r,sec}$	secondary ram drag
D_{spill}	spillage drag
D_{β}	boattail drag
F_g	gross thrust
$F_{g,p}$	primary gross thrust
h,ℓ,x,y,z	distances as defined in figures
L	lift
M	Mach number
M_ℓ	local Mach number
M_s	surface Mach number
M_∞	free-stream Mach number
$\frac{m}{m_\infty}$	inlet mass-flow ratio
p	static pressure
p_t	total pressure
$p_{t,av}$	average total pressure
$p_{t,j}$	jet total pressure
$p_{t,\infty}$	free-stream total pressure
p_∞	free-stream static pressure
q_ℓ	local dynamic pressure

q_∞	free-stream dynamic pressure
R	range
S	wing area
T_j	jet temperature
T_s	surface temperature
T_∞	free-stream temperature
V_A	axial velocity
V_R	rotational velocity
w_p	primary weight-flow rate
w_{sec}	secondary weight-flow rate
$\left(\frac{w_{sec}}{w_p}\right)_{max}$	maximum secondary-to-primary weight-flow ratio
α	angle of attack
β	nacelle toe-in angle; nacelle boattail angle
β_{av}	average boattail angle
δ	thickness of undisturbed boundary layer
δ'	thickness of boundary layer at base of strong shock
η	nozzle efficiency factor
θ	angle between local flow and line parallel to fuselage center line
Λ	wing sweep angle

σ angle of sidewash

ϕ peripheral angle

DISCUSSION

Environmental and Flow-Interference Considerations

The performance of the propulsion system, as always, is critically sensitive to the environment. Items of concern are the characteristics of the airplane flow field, aerodynamic interferences between the airframe and the propulsion package, and jet-airframe interferences.

Flow fields.- Pertinent features of the flow about an isolated inclined body (see refs. 1 to 3) are illustrated in figure 1. The angle θ is the total angle between the local flow and a line parallel to the center line of the body or fuselage, and M_S is the surface Mach number. At an angle of attack of 12^o, as shown by the plots of θ/α and M_S/M_∞, the flow along the bottom of the body aft of the nose region is approximately alined with the local surface and the surface Mach number is decreased from the stream value. The flow across the body results in upflow angles along its sides greater than the angle of attack and in surface Mach numbers greater than the stream value. Accompanying this cross flow is a thickening of the boundary layer at the top of the body, the collection of this boundary layer into lobes along the aft top quadrants, and the formation of twin vortices which entrain much of the thickened boundary layer and then separate from the surface. These phenomena are qualitatively applicable to a strut-mounted nacelle and the section of the fuselage ahead of the wing.

The addition of a wing to the body breaks up the flow across the body and provides a broad sheltered region. Figure 2 presents results of recent NASA surveys of the flow about an arrow-wing configuration at a longitudinal station typical of inlet location for a bomber or transport. (Also see refs. 4, 5, and 6.) The operating conditions chosen are representative of cruising flight for such aircraft. As is discussed subsequently, the most desirable region for locating air inlets generally is beneath the wing-body. The contour plots of M_l and $\partial M_l/\partial\alpha$ in figure 2 show that the local Mach

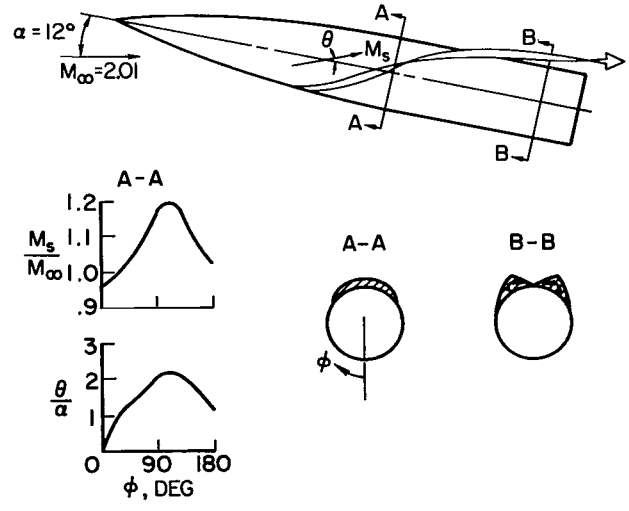

Figure 1.- Pertinent features of flow about an isolated inclined body.

number beneath the wing-body is 0.3 to 0.4 lower than that above the wing-body, and that this advantage of the low position increases rapidly with increasing angle of attack. To be alined with the local flow, a nacelle air intake located in the plane of symmetry would be placed approximately parallel to the body center line. If located under the wing just inboard of the tip, it would be toed in 5° with a 2° down tilt. The rate of change of total flow angularity with angle of attack ($\partial\theta/\partial\alpha$) is less than unity for the entire region beneath the wing and also above the fuselage. Hence, inlets located in these regions experience less severe flow angularity problems than inlets located in the free stream.

Flow-field effects on inlet.- Estimated effects of the flow characteristics just discussed on the pressure recovery at $M_\infty = 3$ of a typical high-performance mixed-compression axisymmetric inlet placed in several locations relative to the airframe are presented in figure 3. Experimental angle-of-attack characteristics of this inlet operating in the free stream, obtained from reference 7, are shown by the dashed curve. Experimental data relative to flow angularity effects on the performance of a wide variety of intake installations are available in the literature (e.g., refs. 3, 8, and 9), but generally are not suitable for the present purpose because of low design pressure recovery or other factors. It is clear that the optimum inlet location is beneath the fuselage in the plane of symmetry. An inlet beneath the wing provides comparable performance over an angle-of-attack range of about 5° in the vicinity of the design value, but suffers significant

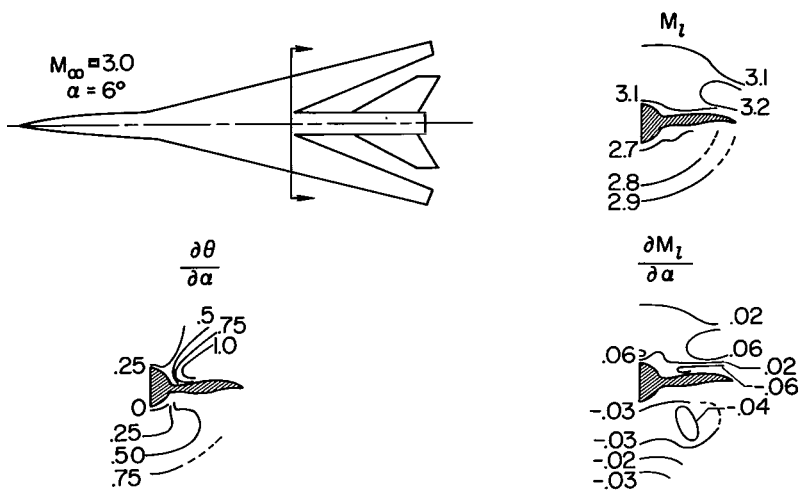

Figure 2.- Flow field for an arrow-wing configuration.

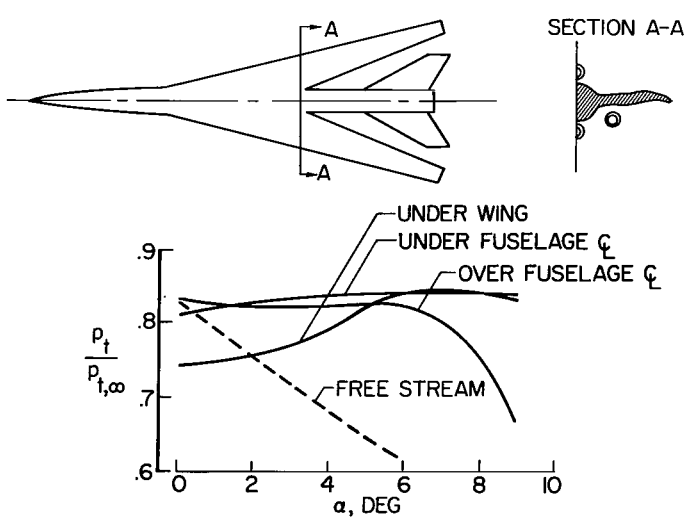

Figure 3.- Effects of flow field on pressure recovery of a typical high-performance mixed-compression inlet. $M_\infty = 3$.

losses outside this range due to the change in sidewash beneath the wing. Surprisingly, an inlet located above the fuselage center line likewise can provide good performance up to cruise angles of attack, and thus it also can be considered as a candidate inlet type for cruise aircraft. Unfortunately, as the angle of attack is further increased, the performance of an inlet located above the fuselage center line deteriorates at a rate even more rapid than does the performance of an inlet located in the free stream, due mainly to the rapid buildup of local Mach number. Its performance also is very sensitive to spanwise location because of rapidly varying flow-field characteristics.

Interference of adjacent surfaces with inlet.- It is well known that the boundary layer plays a major role in determining how close an inlet can be placed to an adjacent surface. As shown by the left-hand plot in figure 4, the pressure recovery of typical inlets (see refs. 3, 8, 10, and 11) increases so rapidly with increases in the lip location parameter h/δ that it is almost always advantageous to locate the inlet entirely outside the boundary layer. It is essential at the same time that the strut or diverter wedge between the inlet fairing and the surface be aerodynamically thin and have its leading edge (or leading edge of the boundary-layer separation plate, if used) located aft of the inlet plane.

The shock—boundary-layer interaction problem may necessitate greater wing-nacelle spacing than that required to optimize pressure recovery at the design condition. Below the design flight Mach number, the nose shock of a center-body inlet passes ahead of the cowl lip and impinges on the adjacent surface. With center-body-nose included angles no greater than 25° or 30° and, for Mach numbers of 3 or less, the strength of this shock is not sufficient to separate a stable turbulent boundary layer, although it may cause some local disturbance and thickening. When the inlet unstarts or buzzes, however, the strength of the shock front may be sufficient to cause boundary-layer separation down to flight Mach numbers approaching 1.3. When such separation occurs, a boundary-layer wedge is formed which greatly thickens the boundary layer at the inlet station.

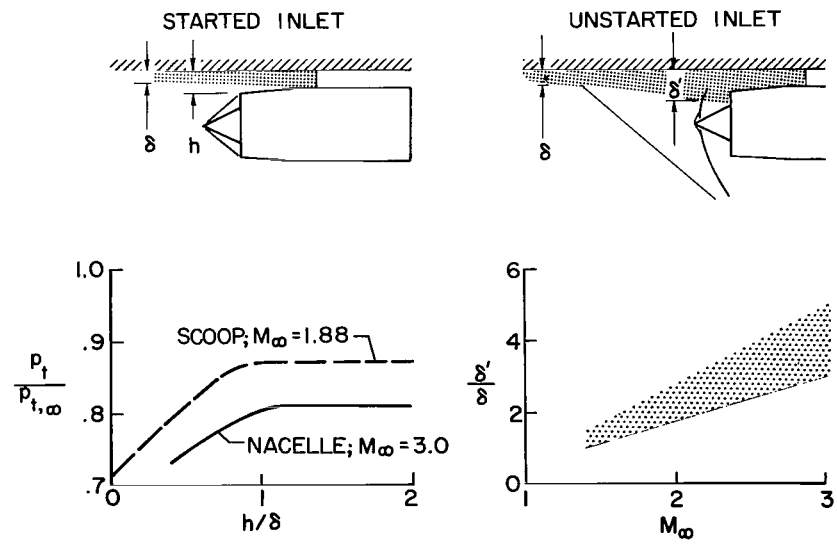

Figure 4.- Role of boundary layer in determining location of inlet relative adjacent surfaces.

The amount of boundary-layer thickening due to separation caused by shock impingement is a complicated function of Mach number, Reynolds number, and other factors (e.g., see ref. 12). The right-hand plot in figure 4 presents results of an attempt to correlate experimental values of δ'/δ as a function of the free-stream Mach number. The width of the band is indicative of the uncertainty that exists at the present time. Additional research is needed to define the phenomena more exactly. However, the conclusion can be drawn that the lip of an inlet of the type shown in figure 4 must be separated from the surface by a distance several times greater than δ to avoid some of the separated boundary layer from entering the inlet and thereby complicating the restart process. An alternative solution might be the use of a horizontal-wedge inlet oriented so as to direct the ramp shocks away from the adjacent surface or a vertical-wedge inlet mounted beneath a boundary-layer separation plate. The recent flight research finding that an unstart of one side of the XB-70A inlet frequently initiates an unstart of the other side raises questions concerning the soundness of such approaches. The time interval of 3 to 4 seconds observed between such successive unstarts indicates, however, that the problem in this particular instance probably is occasioned by airplane motions accompanying the initial unstart or other factors rather than by interactions between the left-hand and right-hand inlet shock systems. Thus, consideration of this general approach cannot be discarded at this time.

Mutual interference of adjacent inlets.- In a multiengine installation it is important to separate the inlets sufficiently so that the unstarted bow wave of one inlet will not enter and cause the unstarting of adjacent inlets. Figure 5 presents a compilation of spacing requirements data, obtained mainly from references 13 and 14, for high-performance mixed-compression inlets with the forward inlet buzzing and the rearward inlet operating at high pressure recovery. At $M_\infty = 3$ and with the inlets located abreast, separation of about $1\frac{3}{4}$ inlet diameters appears to be ample. However, when the inlets are staggered, as is desirable from the drag minimization viewpoint, the separation distance required increases markedly. In extreme cases, some sort of separation plate, such as is discussed in reference 13, may be required to arrive at a practical configuration arrangement.

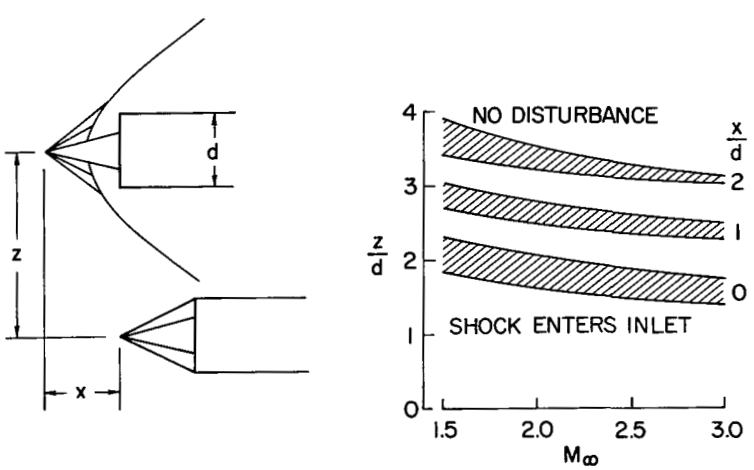

Figure 5.- Spacing requirements for high-performance mixed-compression inlets (forward inlet in steady-state buzz). $M_\infty = 3$.

Two reservations concerning the applicability of the

data in figure 5 for design purposes must be noted. First, the travel of the initial unstart bow wave and the buzz amplitude of the configuration being considered may differ from those for the models studied because of the different system dynamic characteristics. Second, if the inlets under consideration are located close to an airplane surface, the nature of the mutual interaction between the two inlets will be modified by shock—boundary-layer interaction effects at the airplane surface. Reportedly, in extreme cases, the separation requirements may be nearly doubled. At the present time, the designer has no recourse but that of further experimental study to insure avoidance of trouble.

Inlet separation requirements.- Although there are installations such as that of the XB-70A in which two or more engines are fed by a single duct, the current trend is to separate the intake flows to the greatest extent possible. The Concorde reportedly uses a splitter plate to separate its two-dimensional inlet into two parts. In figure 6 is shown a similarly split three-dimensional inlet designed for a Mach 2.5 airplane. In both cases, the prime requirement of the plate is that it prevent the unstarting and buzz of one side of the inlet from affecting the other side.

Experimental studies were conducted by NASA (see ref. 15) to establish splitter-plate requirements of the nacelle arrangement illustrated in figure 6. As shown by the sketch at the lower left of the figure, the model used incorporated an inlet fully represented on one side of the separation plate but replaced by rapid-response total-pressure probes on the other side. In the tests, buzz was initiated in the ducted side of the plate by reducing the duct exit area. Oscillograph traces of the pressure fluctuations measured by the probes on the other side of the plate then were observed to determine whether or not the flow on this side of the plate was affected. It was found that there was no measurable interaction so long as the inlet was located well away from the wing and so long as the splitter plate extended to the nose of the inlet center body and, in the plane of the inlet, was about $7\frac{1}{2}$ percent wider than the inlet diameter. On the right-hand side of figure 6, a satisfactory splitter plate and corresponding oscillograph traces are shown in the top sketch. When the same nacelle model was moved nearer the wing (see middle sketch), extensive interaction occurred due to shock—boundary-layer interaction accompanied by crossfeeding of disturbance pressures through the gap between the plate and the

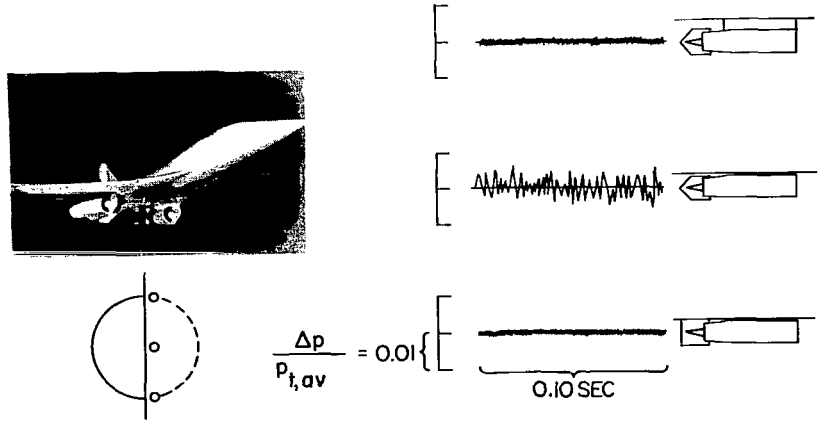

L-2614-15

Figure 6.- Splitter-plate requirements for twin-pod inlet. $M_\infty = 2.5$.

wing. Sealing the gap between the separation plate and the wing eliminated this cross-feeding (see bottom sketch). Thus, a properly designed separation plate would appear capable of effectively isolating the two inlet flows provided the initial unstart shock front does not impose conditions more severe than those studied. Again, further experimental studies are needed.

Jet-airframe interference.- Basic jet phenomena (see refs. 16 and 17) are illustrated in figure 7. At subsonic flight speeds and with a convergent nozzle or an underexpanded convergent-divergent nozzle, the jet expands through a series of internal Mach diamonds that do not penetrate the jet boundary. The edge of the jet is a mixing region. The jet acts as a weak sink causing an inflow of air from the external stream toward the jet axis. The jet itself is not a rigid body, but undergoes deflections due to aerodynamic forces at high angles of attack and in the presence of the ground. At supersonic speeds, inflow effects generally are negligible, but the expansion process within the jet produces an external shock system that affects adjacent surfaces. Jet deflection effects tend to be more pronounced than at subsonic speeds because the ratio of the jet dynamic pressure to the free-stream pressure is much lower.

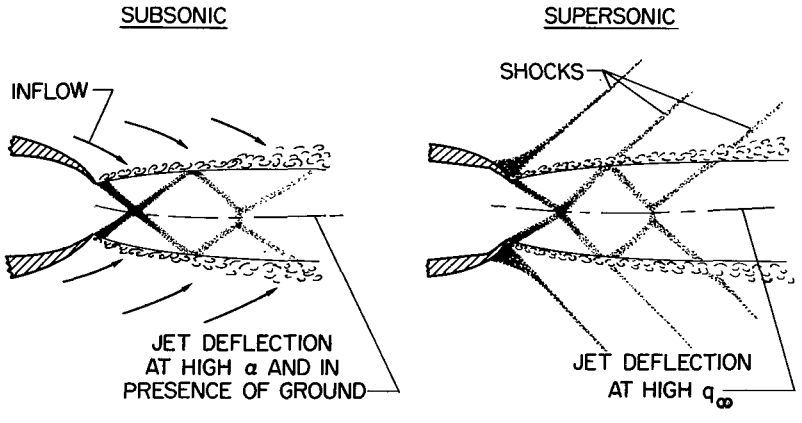

Figure 7.- Basic jet phenomena.

Jet interference effects greatly complicate the jobs of the aerodynamicist, the loads engineer, and the structural designer. An NASA jet-effects investigation of a twin-engine fighter model, reported in part in reference 18, affords a good illustration of typical problems encountered at subsonic speeds. In figure 8 is plotted the normal-force coefficient for the horizontal tail, obtained by integration of pressure measurements on the tail, as a function of angle of attack. For the high tail position,

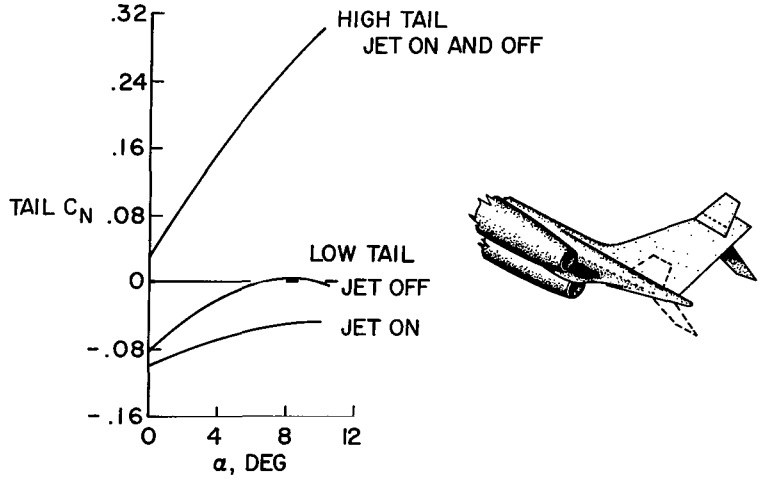

Figure 8.- Jet interference effects on tail normal-force ceofficient of a twin-engine fighter model. $M_\infty = 0.85$; $p_{t,j}/p_\infty = 5$.

there was no effect of jet operation on the tail forces. When the tail was moved to the low position, indicated by the dashed lines on the sketch in figure 8, the curve for C_N as a function of α was shifted and rotated in a destabilizing direction, as would be expected as a consequence of the position of the wing wake and the change in downwash at the tail location. In addition, at this low tail position, operation of the jet produced both an additional shift and an additional destabilizing rotation of the curve. Further important changes have been observed when the tail of an airplane of this general configuration is located close to the ground or when the tail is deflected sufficiently so that its leading edge penetrates the jet boundary.

Figure 9 presents temperature and static pressure distributions on the afterbody of the same model. For a jet pressure ratio of 5, which is applicable to some future high-pressure-ratio engines, the pressure-distribution curve exhibits a succession of peaks and valleys which are related to the expansion process within the jet and indicate jet attachment. For the lower jet pressure ratio of 2.7, which is typical for most present engines, the jet was no longer attached. Even at this operating condition, the temperature rises along the afterbody were of sufficient magnitude to eliminate the use of aluminum as a structural material. Likewise, although the static loadings imposed on the afterbody by jet operation were small in themselves, they were accompanied by pressure fluctuations of sufficient magnitude to affect the fatigue life of the structure. A number of configuration changes were investigated to explore means for reducing the severity of these adverse jet effects. The most successful was the introduction of secondary flow into the base areas between the jet nozzles and the afterbody (compare short- and long-dashed curves in fig. 9). The design solution adopted involved the use of significant quantities of secondary flow, high-temperature surface materials, and well-damped structural panels. Obviously a less costly design solution would be desirable.

Figure 10 shows how the nature of the jet interference problem changes as the flight speed progresses from the subsonic to the supersonic regime. Incremental static loadings (sum of upper and lower surface pressure-coefficient changes) induced on a 60° delta wing by the jet

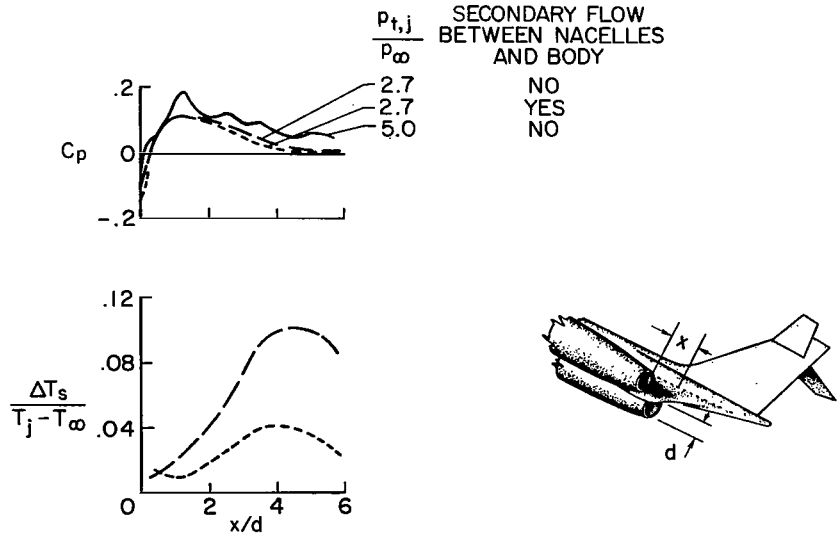

Figure 9.- Jet effects on afterbody of a twin-engine fighter model. $M_\infty = 0.85$; $\alpha = 4^0$.

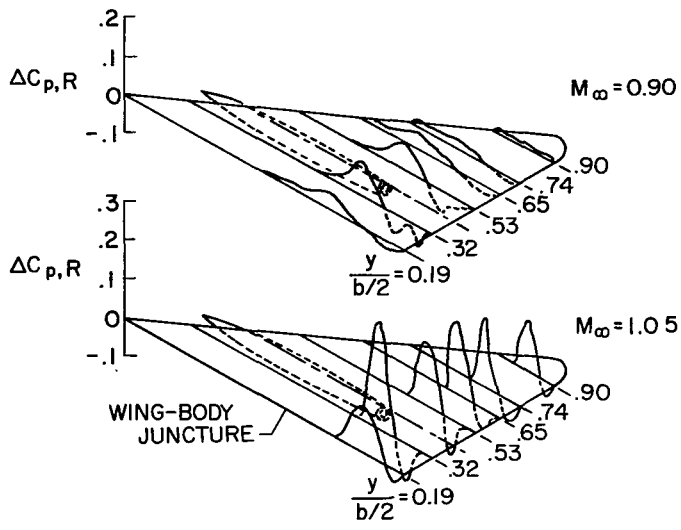

Figure 10.- Jet-induced pressures on a 60° delta wing. Exit located 1 exit diameter below the wing at $\frac{y}{b/2} = 0.41$ and 69% chord; $\alpha = 5^\circ$; $p_{t,j}/p_\infty = 5$.

exhaust of a nacelle located beneath the wing are plotted for flight Mach numbers of 0.90 and 1.05. (See refs. 19 and 20.) At both Mach numbers, the angle of attack was 5° and the jet pressure ratio was 5. For the subsonic speed, both upper and lower surface pressures were affected by jet operation, with the greatest changes occurring on the lower surface in the immediate vicinity of the jet exit. For the supersonic speed, in contrast, all the pressure changes occasioned by jet operation occurred on the lower surface. A strong shock generated by the jet plume completely spanned the wing and produced significant changes in pitching moment, control effectiveness, drag, and wing loads. As the Mach number was further increased, this shock swept back rapidly and caused further variations in interference characteristics.

The jet interference effects considered in this discussion of figures 8 to 10 cannot be predicted accurately for complex configurations by available theoretical methods. For the most part, the designer is forced to rely on empirical correlations or model tests. The need for continued research in this area is evident.

Integration of Propulsion System With Airframe

New analytical tools.- The development of machine computing techniques has provided the designer with powerful new tools for optimizing the aerodynamics of the vehicle. The increase in capability has been particularly great in the supersonic regime where efficient vehicles must be aerodynamically slender so that linear theory methods may be used.

In early applications of area-rule methods for the purpose of minimizing the zero-lift wave drag, it was necessary to obtain the many required area cuts by graphical or semigraphical methods. Now, most manufacturers have computer programs that eliminate this drudgery. (See ref. 21.) As indicated in the left part of figure 11, the engineer provides the computing machine with data defining the cross-sectional areas of the fuselage and nacelles as functions of fuselage station, data defining the airfoil coordinates of the wing and tail as functions of spanwise station, and coordinates defining where the forward points of components other than the fuselage are located relative to the fuselage.

The machine then takes over the task of calculating the areas intercepted by "Mach planes", of making area distribution plots for each cutting plane, and finally of fairing the area curves and determining the overall pressure drag. As shown in the right part of figure 11, good correlation has been obtained between computed and experimentally determined values for a large number of configurations and for a wide range of Mach numbers.

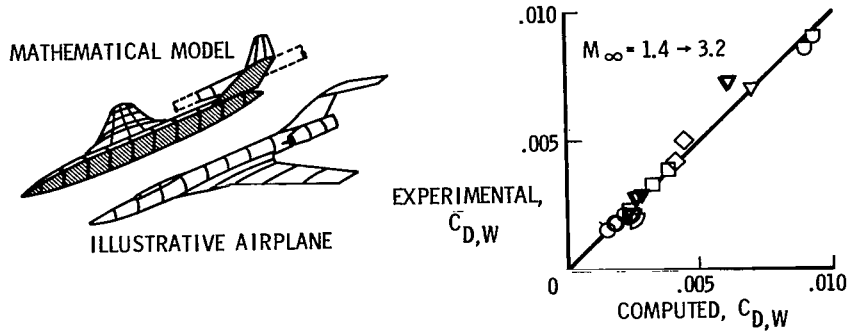

Figure 11.- Zero-lift wave drag.

Another important application of the high-speed computer has been in the calculation of the optimum wing surface shape for arbitrary planforms and loadings and, conversely, in the calculation of pressure distributions on arbitrary wings. (See refs. 22 and 23.) This capability has made practical the previously staggering task of calculating the drag due to lift, camber drag, pitching moments, aerodynamic loadings, and so forth, and has permitted the aerodynamicist to play an effective role in the preliminary design process. It also has cleared up some long-standing mysteries. For example, although theory has long indicated that a properly warped wing with a subsonic leading edge should provide significantly lower drag due to lift than its flat counterpart, the predicted gains were never fully realized in practice. As shown in the left-hand plot in figure 12, the experimental points fell well below the long-dashed curve corresponding to flat-wing theory but still significantly above the solid curve predicted for the warped

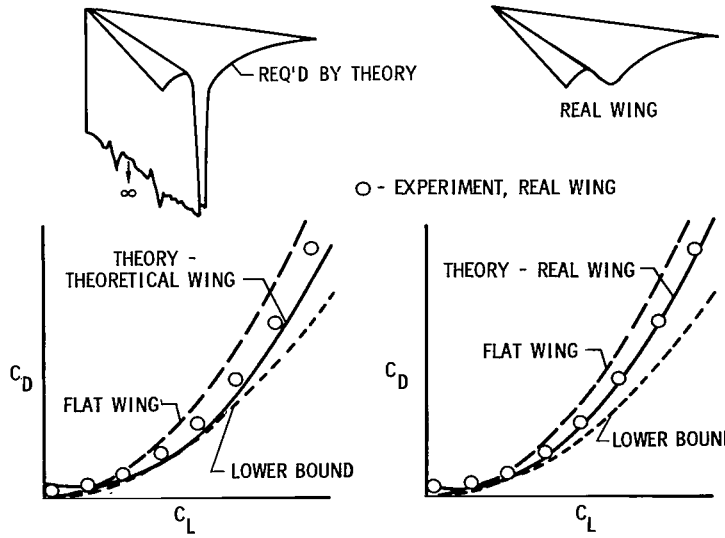

Figure 12.- Drag due to lift of real and theoretical wings. Design $C_L = 0.08$; $\Lambda = 70^0$; $M_\infty = 2.05$.

wing. The main reason for this discrepancy is that the theoretical model required infinite slopes at the wing root (see left-hand sketch), whereas the model wing necessarily incorporated finite surface slopes in this region (see right-hand sketch). When the new machine computing techniques were utilized to calculate the pressure distribution on the real wing shape rather than on the previously used theoretical model, the discrepancy between theory and experiment essentially was eliminated. (See right-hand plot in fig. 12.) Good correlation between theory and experiment now is being obtained for a wide range of wing planforms.

Nacelle shape, size, and location effects.- The analytical tools just discussed have been used by Boeing (ref. 4), NASA (ref. 24), and others to study the effects of major nacelle design and installation variables on the increments in wave drag chargeable to nacelle installation. Boeing calculations presented in figure 13 show typical shape and size effects for nacelles placed on an arrow-wing airframe in a near-optimum location. Wing lift coefficient is used as the abscissa of the nacelle wave-drag-increment plot inasmuch as interference effects are a sensitive function of the Mach number and sidewash beneath the wing. Boattailing of the nacelles was found to increase significantly the drag due to the nacelles at cruise lift coefficients, as would be expected from consideration of its effect in reducing the local pressures on the aft part of the nacelles and on the adjacent wing surfaces. Conversely, NASA calculations indicate that flaring the nacelle forward of the wing trailing edge has a pronounced favorable effect due mainly to the favorable interference effects on the wing. Thus, the ideal shape for a nacelle would appear to be a truncated cone rather than a cylinder as is frequently assumed.

Increasing the nacelle dimensions as much as 20 percent likewise was found to reduce the overall pressure drag at and above the usual values of cruise lift coefficient. At first, this result appears inconsistent, but it can be explained readily by the large favorable interference effects. Confirmation of this general trend of reduction in drag

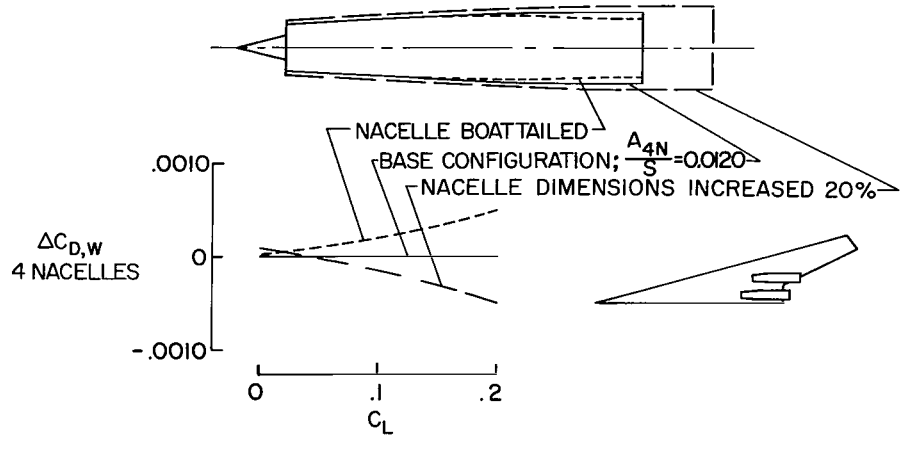

Figure 13.- Calculated effects of nacelle shape and size on wave drag. $M_\infty = 2.7$.

with increase in nacelle size is provided by the NASA experimental data presented in figure 14. The drag coefficients shown are the total external pressure plus skin-friction drag increments measured when four nacelles were added to a basic wing-body configuration. The large nacelles had higher drag than the small nacelles in the lower range of lift coefficient; however, the curves cross at a lift coefficient of about 0.1 so that the larger nacelles had lower drag in the cruise and climb ranges. These curves provide a dramatic illustration of the sensitivity of interference effects to the flow conditions beneath the wing. It is emphasized that these results are quantitatively applicable only to arrow-wing configurations with near-optimum nacelle locations. Interference effects would be expected to be different for other wing planforms and other nacelle locations.

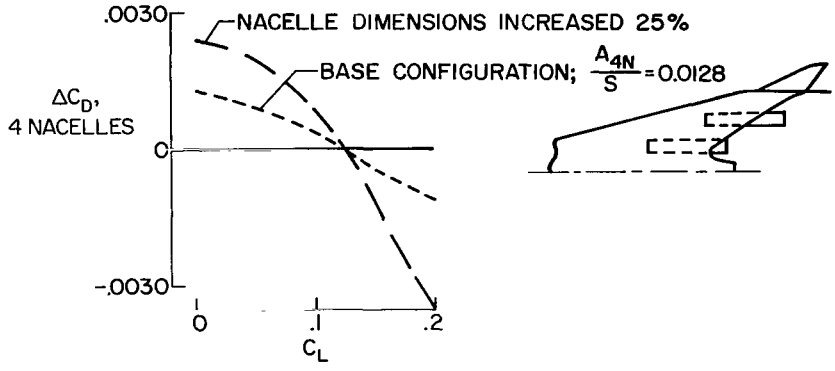

Figure 14.- Experimental effects of nacelle size on overall drag. $M_\infty = 2.6$.

Calculated effects of nacelle longitudinal location on the wave drag increment due to installation of nacelles on the arrow wings just discussed are presented in figure 15. For convenience of interpretation, the wave drag increment is related to the calculated wave drag increment for four isolated nacelles. The abscissa of the curve is the distance of the lip of the most forward nacelle from the most forward point in the wing notch expressed in terms of the nacelle diameter. The stagger of the inboard and outboard nacelles and their spanwise spacing were maintained constant in the study. At each longitudinal location, the basic wing-body was shaped to

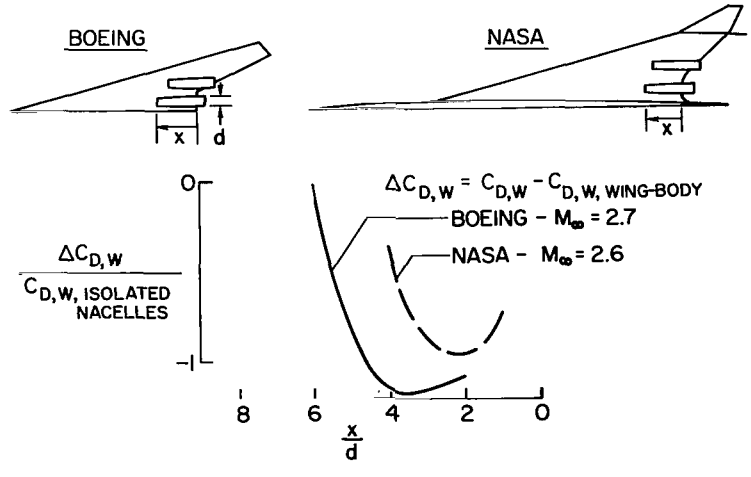

Figure 15.- Calculated effects of nacelle location on wave drag.

account for the presence of the nacelles. Hence, even for the most forward location which is the most unfavorable position considered (see left end of solid curve), addition of the nacelles to the wing-body was accomplished with no increase in total wave drag. The effect of moving the nacelles rearward from the most forward location was to provide significant further decreases in the wave drag. At the optimum location, the maximum additional reduction is indicated to be approximately equal to the calculated total wave drag of the isolated nacelles. These results emphasize the fact that interference effects play a dominant role in determining the aircraft drag and cannot be neglected or ignored in the design process.

Integration of nacelle with wing.- In order to take maximum advantage of favorable interference effects, close attention must be paid to local details of the nacelle and the adjacent wing surfaces. The addition of the nacelles to the wing imposes overlapping regions of positive pressure on the wing lower surface. (See upper sketch in fig. 16.) As discussed in reference 24, the magnitude of these pressures can be estimated by the method of characteristics or the modified linear theory of Whitham. With the lift characteristics of the local surface defined, the wing camber surface then can be reflexed locally, as illustrated in the lower sketch in figure 16, to restore the wing load distribution in this region to its design value. The effective result is a reduction, in the reflexed region, of the slopes of both the top and bottom wing surfaces relative to the stream direction. These reductions in surface slope reduce the pressure drag associated with the reflexed part of the wing and, as shown in the data plot, produce major improvements to the drag polar.

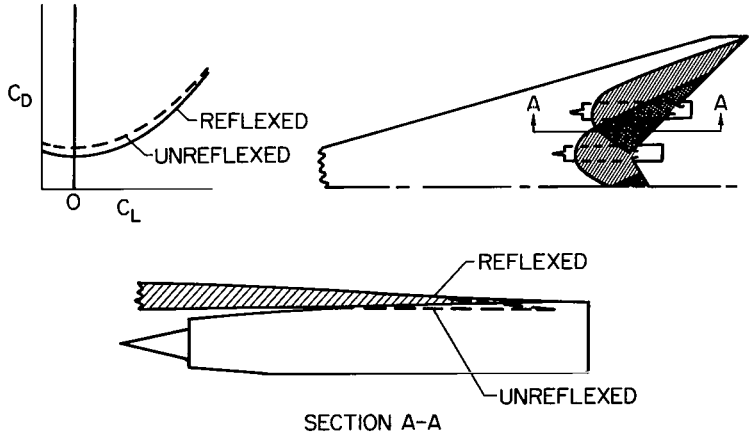

Figure 16.- Use of wing reflex to accommodate nacelle interference. $M_\infty = 2.6$.

It was noted previously that the nacelle drag increment is sensitive to changes in the wing lift coefficient due to accompanying changes in Mach number and sidewash beneath the wing. The drag, therefore, might be expected to be sensitive also to the toe-in angle of the nacelle. Figure 17 presents experimental results obtained by NASA at

$M_\infty = 2$ and $C_L = 0.16$ for an arrow-wing configuration with simulated nacelles located at one nacelle radius below the wing. The experimental results are shown to be in good agreement with calculations made in accordance with the theory outlined in reference 25. The drag increment of the two nacelles varied about seven airplane drag counts as the nacelle toe-in angles were varied from -4° to 8°. In accordance with the theory of reference 25, minimum drag occurred when the nacelles were toed in at approximately one-half the local sidewash angle. This toe-in angle usually differs slightly from the toe-in angle necessary for alining the inlet precisely with the local flow, so a compromise setting or a bend in the nacelle may be desirable.

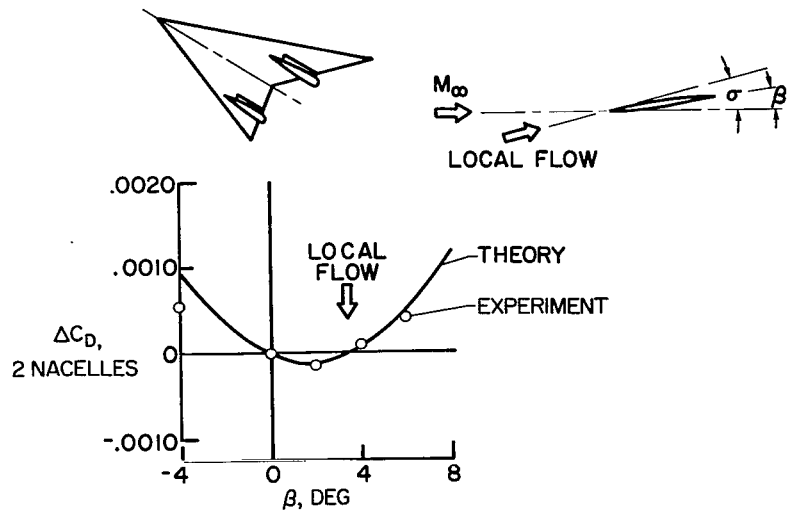

Figure 17.- Optimization of nacelle alinement. $M_\infty = 2$; $C_L = 0.16$; $\frac{A_2 N}{S} \approx 0.007$.

Propulsion System Optimization

The design of the propulsion system itself is necessarily carried out in close coordination with the process of integrating it into the overall configuration. Figure 18 is included to provide an appreciation for the relative importance of the major installation considerations. Presented in this figure are range increments calculated for a typical Mach 2.7 transoceanic supersonic transport, with parameters varied in the cruise leg of the mission only. The performance of the airplane in other legs of the mission is affected similarly, of course, by changes in the same parameters, but to a different extent. Small changes in inlet pressure recovery, propulsion package weight, lift-drag ratio, and nozzle gross-thrust coefficient all are shown to have significant effects on range capability, with their importance increasing in the order in which they are listed. As a result, propulsion systems designed for supersonic cruise aircraft (see fig. 19) typically incorporate variable-geometry components and complex secondary-flow systems in order to optimize performance over the wide range of operating conditions encountered. This section of the paper includes a discussion of component characteristics from an installation or systems viewpoint, the problem of optimizing the handling of the major secondary flows during supersonic operation, and afterbody drag.

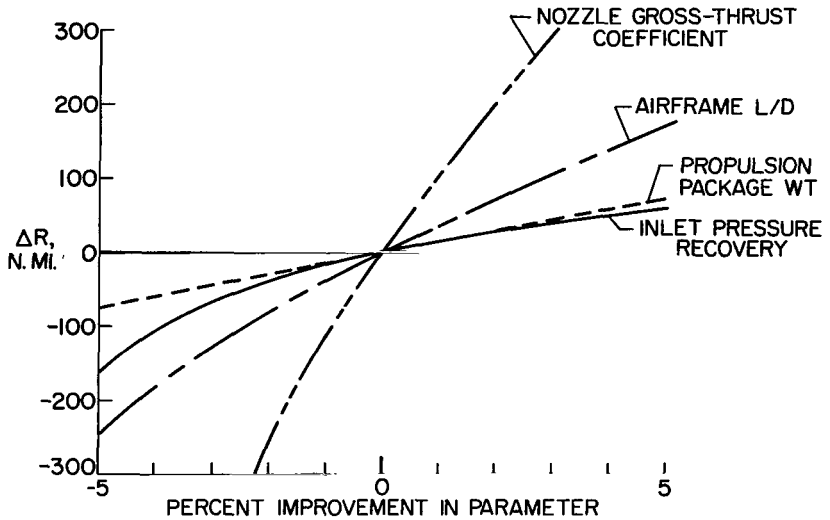

Figure 18.- Performance sensitivity of propulsion-system installation for a typical supersonic transport. M = 2.7 cruise; 3500 n. mi. mission.

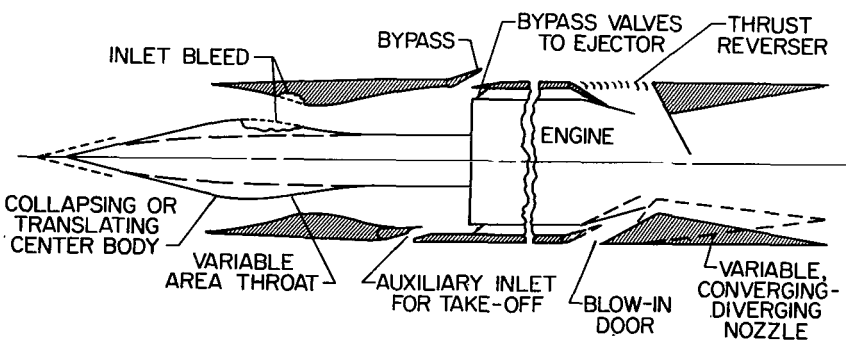

Figure 19.- Features of propulsion systems of supersonic cruise aircraft.

Inlet characteristics.- Inlet pressure recovery continues to be a subject of major interest to the designer. However, as indicated in figure 18, other factors such as the nozzle gross-thrust coefficient and the airframe L/D tend in many cases to be more critical from the overall performance viewpoint. At the same time, inlet weight, starting characteristics, control characteristics, flow stability characteristics, and flow distortion characteristics frequently present more difficult design and developmental problems. As a result, such factors frequently are assigned an importance equal to or greater than that of pressure recovery in the inlet selection process.

The three basic inlet types of principal interest for airplanes at Mach numbers from 2.5 to 3 are illustrated in figure 20. At the present time design applications of all three types of inlets generally feature fixed cowl lips to minimize cowl weight. Variable throat area and variable supersonic compression geometry are incorporated to accommodate starting, off-design operation, and control requirements. Shown below the sketches are typical plots of pressure recovery as a function of mass-flow ratio for the design Mach number. For each inlet type, the solid and dashed lines represent the regions of stable and unstable operation, respectively, and the circular symbol indicates a typical design operating point. The portion of the solid line to the left of the symbol is the stability margin either available or required as the case may be.

The external-compression inlet is the shortest and lightest of the three inlet types. Inasmuch as it has no internal contraction, it is inherently self-starting and can have a wide stability margin. Unfortunately, its peak pressure recovery is much lower than for the other types and, for the higher Mach number designs, the large external turning requirements necessitate rather large external lip angles with attending high cowl drag. Hence, it is seldom considered for applications involving protracted operation at Mach numbers above about 2.2.

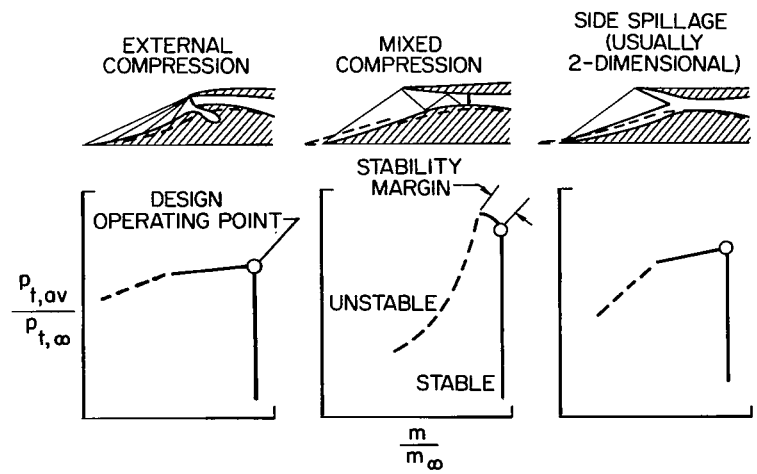

Figure 20.- High-performance inlet types.

The mixed-compression inlet affords the potential of very high peak pressure recovery and low external drag at the expense of increased complexity and weight. The terminal shock cannot be stabilized in the contracting region between the cowl lip and the inlet throat. Consequently, since the amount of internal contraction used is large, reductions in mass-flow ratio below the value corresponding to peak pressure recovery cause a drastic drop in pressure recovery and initiate flow instability. Hence, the design operating point must be located 3 to 5 percent below the peak pressure recovery point to insure the avoidance of unstarts due to external disturbances and to allow for the inability of the control system to hold the terminal shock very close to the throat position. In addition, substantial variations in inlet geometry are required to reestablish the design operating conditions should an unstart occur. In brief, this type of inlet affords the highest performance of the three basic types, but at the same time poses the most difficult flow stability and control problems.

Several American companies are studying so-called self-starting mixed-compression inlets. In one kind, the amount of external compression is increased at the expense of some increase in external cowl angle and the amount of internal contraction is reduced sufficiently to permit reestablishment of the supersonic flow following an unstart without the necessity for varying the throat geometry. In a second kind, the inlet bleed system is designed to provide a recirculation of the bleed flow when the normal shock moves ahead of the inlet throat. The flow enters the surface behind the shock where the static pressure is high and exits from the surface ahead of the shock where the static pressure is lower. Hopefully, this recirculation thickens the boundary layer at the lip station and thins it at the throat thereby reducing the effective internal contraction and permitting automatic restarting. If perfected successfully, either kind of self-starting inlet may provide a good compromise between the relatively tractable external-compression inlet and the higher performance but less easily controlled mixed-compression inlet.

The third basic type of inlet illustrated in figure 20 is essentially a two-dimensional internal-contraction inlet with sidewalls cut back to permit spillage during the starting process. It can be designed to provide high pressure recovery and low drag for the design operating condition, as well as a significant degree of subcritical stability. Its weight and sensitivity to flow angularity are expected to be problems, but these problems may be overbalanced for many applications by its desirable flow stability and restart characteristics.

Distortion and unsteadiness of inlet flow.- One of the major problems of the propulsion-system designer is that of maintaining a low level of distortion and unsteadiness of the flow at the engine throughout the operating envelope of the airplane. These phenomena, which are discussed in many references (e.g., refs. 3, 8, 9, and 11), are a

complicated function of a very large number of variables, some of which are flow inclination at the inlet, boundary layer of adjacent surfaces, external shock interference, vorticity and flow separation associated with subcritical inlet operation, inlet unstart and buzz, and inadequate mixing length in the inlet throat and in the subsonic diffuser. Other sources of distortion and unsteadiness include nonuniformity of air removed or inducted through the duct walls (e.g., through bypass or auxiliary take-off passages), inability of the control system to maintain the inlet terminal shock at a fixed station in the presence of atmospheric, engine, and control transients, and disturbances propagated forward through the engine and nacelle secondary-flow passages.

A detailed discussion of the many sources of flow distortion is beyond the scope of this paper. It is instructive, however, to take a look at the basic mechanism (see ref. 11) through which distortion of a steady flow affects engine performance. Consider in figure 21 the front rotor-blade row of the engine, where V_R is the rotational velocity, V_A is the local airflow axial velocity, and α is the local blade angle of attack. If local total pressure losses reduce V_A, α increases in the direction of blade stall. On the other hand, if the local flow velocity is increased above the mean value, α and thus the corresponding local pressure rise through the blading are reduced, with the reductions tending to promote choking further aft in the compressor. The importance of these effects depends on the magnitude and extent of the flow distortions involved as well as on the tolerance of the engine to such distortions. For a nonsensitive engine both small-magnitude radial distortions and small-magnitude circumferential distortions of small angular extent tend to wash out in succeeding blade rows. For greater flow distortion, or for a more sensitive engine, however, the distortion frequently carries completely

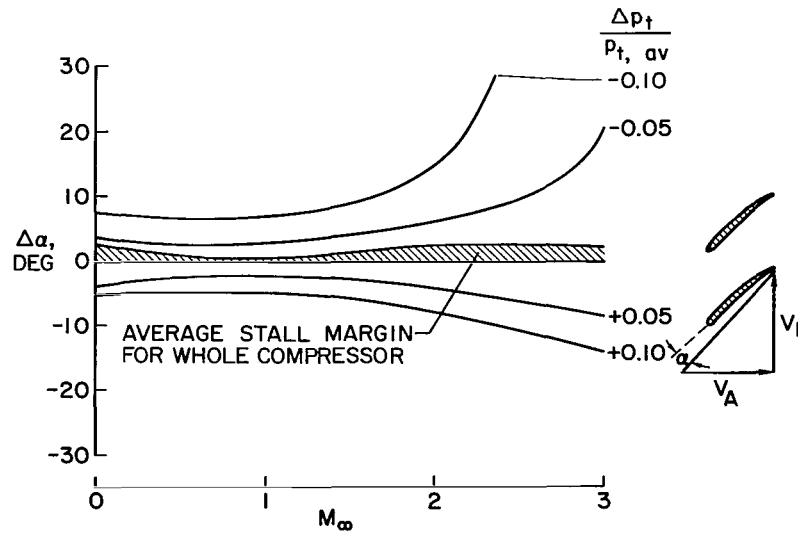

Figure 21.- Problem of allowable flow distortion.

through the compressor and produces hot spots in the combustor and turbine. Combustor flameout, compressor surge, and even structural damage to the engine may result.

Engine manufacturers frequently express their estimate of the allowable flow distortion for an engine in terms of an area weighted deviation of the total pressure in local regions from the overall average. Effectively this way of specifying distortion tolerance is equivalent to assuming that the total pressure variation is indicative of the flow velocity distribution and, hence, of the angle-of-attack distribution along the front blade row. It is not always appreciated that this assumption is somewhat misleading. For example, the plot in figure 21 shows local blade angle-of-attack increments calculated for a Mach 3 turbojet for deviations of 5 and 10 percent in the local total pressure from the overall average. Even for 5-percent distortion, the local blade angle-of-attack changes are very large compared with the average available stall margin; also the magnitude of the local angle-of-attack change is a pronounced function of free-stream Mach number. Two conclusions are evident. First, a distortion parameter is required that is more representative of the actual flow phenomena and, second, the flow-distortion problem tends to become more critical at the higher Mach numbers.

At the present time the propulsion-system engineer tries to handle the flow distortion problem by placing the inlet in a favorable location, alining it carefully with the flow, allowing generous flow mixing lengths, conducting extensive model flow distribution tests, and so forth. Almost invariably these efforts are not sufficient and a cut-and-try development effort is required on the prototype. Extensive research is needed to better understand the flow distortion problem, to develop better flow distortion criteria, and to find ways of both improving the uniformity of the flow delivered by the inlet and of reducing the flow distortion sensitivity of the engine.

Nozzle characteristics.- Calculated performance trades such as those presented in figure 18 show that a high level of nozzle efficiency is mandatory for supersonic cruise aircraft. Most current designs use various forms of the ejector nozzle such as those depicted in figure 22 because a certain amount of engine cooling airflow is always required.

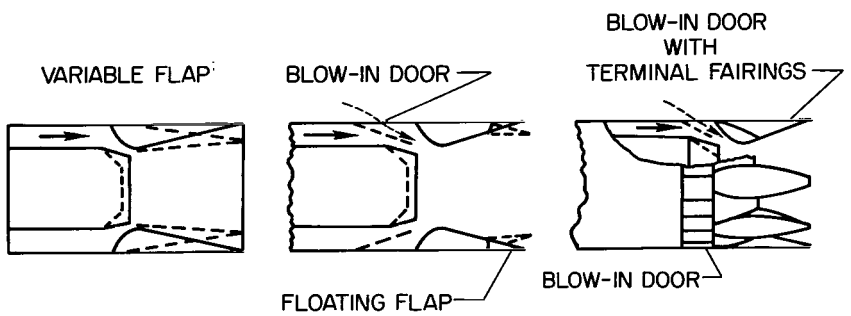

Figure 22.- High-performance ejector nozzles.

The variable-flap converging-diverging nozzle currently being utilized on the B-58 and XB-70A airplanes is the most versatile form inasmuch as both the internal and external shroud surfaces can be varied to optimize its performance. (See refs. 26, 27,

and 28.) With no geometric restrictions, the nozzle can be designed to provide 98 to 98.5 percent of the ideal internal gross thrust for flight Mach numbers up to 3. In an actual design, however, the drag of the external shroud surface must be considered and the use of "practical" linkage arrangements invariably leads to compromise of the internal shroud shape at off-design operating conditions. The net result, illustrated in figure 23 for the case of typical convergent-divergent ejector nozzles designed for a supersonic transport, generally is a deterioration of performance in the off-design operating conditions relative to the ideal value. Such losses tend to be large in the low supersonic range where the thrust minus drag margin is a minimum. Hence, the various trades involved in the design of such a nozzle must be studied carefully. The exercise of design ingenuity frequently can provide important gains in overall mission performance.

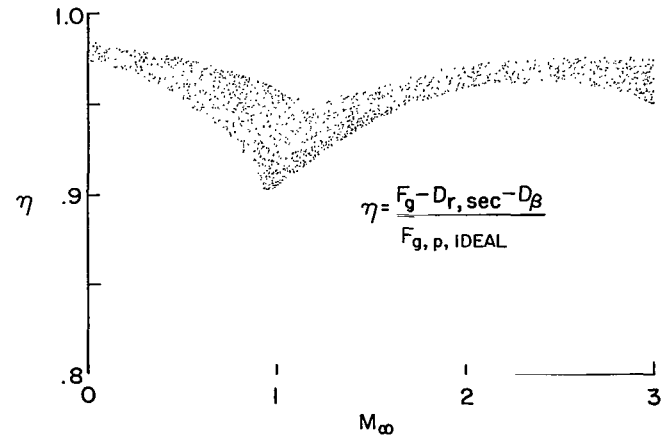

Figure 23.- Predicted maximum performance of convergent-divergent ejector nozzles designed for a typical supersonic transport mission.

The "blow-in-door" nozzle portrayed in the middle sketch in figure 22 is currently being applied to a number of new aircraft. Design simplification is achieved and weight reductions obtained by the use of fixed geometry throughout most of the internal and external shroud surfaces. Blow-in doors, which are closed in high-speed operation but which open to provide increased secondary flow when internal shroud pressures are low, and floating flaps, which provide some variation in shroud exit area, are incorporated in the design to provide a level of nozzle performance approaching but obviously not quite equaling that of the variable-flap ejector nozzle. One problem that must be solved in each application of the blow-in-door nozzle is that of locating and proportioning the blow-in doors in such a manner that an acceptable distribution of blow-in-door flow will be obtained under all important flight conditions. Pressure distributions measured on the afterbody of a twin-engine fighter research model (fig. 24) indicate that this is sometimes a difficult task. For the particular model considered, the pressure distributions along different meridians of the afterbody differed significantly because of the presence of the fuselage and the tail surfaces. Further, these pressures changed with changes in flight condition and tail deflection and were everywhere lower than those measured for similar locations on a geometrically similar isolated nacelle. Hence, a major concern of the designer is the fact that operational characteristics estimated on the basis of test results for a simplified model may be misleading.

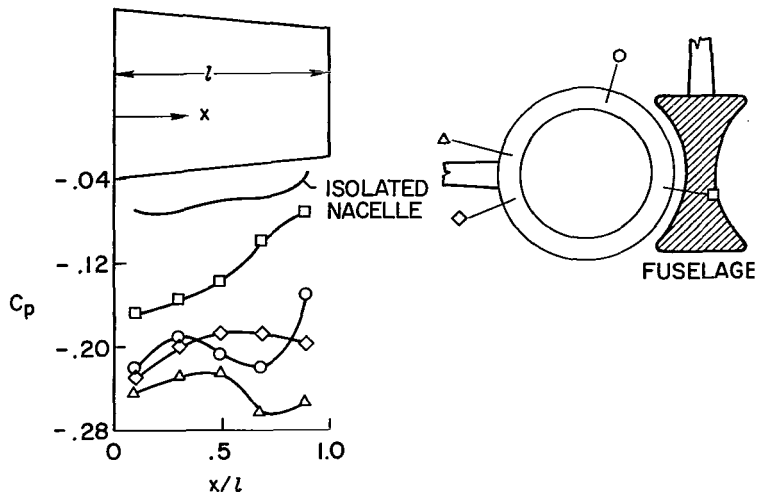

Figure 24.- Pressure distributions measured on afterbody of twin-engine fighter. Jets operating; $M_\infty = 1.2$.

The nozzle shown in the right-hand sketch in figure 22 incorporates a further possible design simplification being studied currently by NASA. Essentially, the aft part of the shroud and the floating flaps of the blow-in-door nozzle are replaced by terminal fairings (see ref. 29), which provide a ventilated shroud afterbody. At low internal pressure conditions, the external flow can enter the slots and prevent overexpansion of the internal flow. Conversely, at high internal pressure conditions, the internal flow can expand outward through the slots and provide increased thrust by reacting against rearward sloping surfaces. Shock—boundary-layer interaction phenomena permit the surface pressures to be increased on the boattail areas ahead of the slots as well as on the terminal fairings only. Information obtained to date indicates that this type of nozzle can provide good off-design performance; however, its design-point performance again would not be expected to equal that of the variable-flap design.

From the performance viewpoint the jet nozzle is by far the most critical installation component. All possible avenues for further increasing its efficiency must be explored, including the possibility of exploiting favorable external-internal flow interference effects.

Handling of secondary nacelle airflows.- The basic nature of the inlet-engine airflow matching process has been treated in so many references (e.g., refs. 3, 11, and 30) that it will not be discussed further herein. However, a typical airflow matching plot for a supersonic transport is shown in figure 25 to illustrate the magnitude of the secondary airflows that must be handled by the installation. From the viewpoint of optimization of the overall installation for high-speed operation, the airflows of principal interest are the inlet spillage flow, the overboard bypass flow, and the bypass flow to the ejector. The inlet bleed flow (see refs. 3, 7, 8, 9, 10, and 11) obviously also is subject to design optimization, but is so closely tied to the inlet performance question that it is considered to be a separate subject outside the scope of this paper.

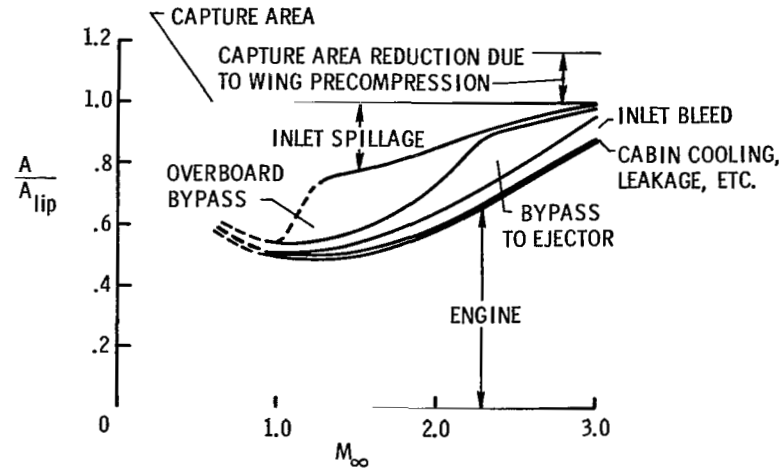

Figure 25.- Typical inlet-engine airflow matching plot.

For a center-body inlet, spillage occurs as the Mach number is reduced below the design value because of the movement of the center-body shock ahead of the cowl lip. Figure 26 presents a calculation, obtained by the general method described in reference 31, of the amount of and drag of the spillage flow for Mach 3 center-body inlets during supercritical operation, which is the condition necessary for minimizing the spillage drag. (Also see refs. 3, 8, 9, and 11.) In this figure, A_{xs}/A_{lip} is the ratio of the stream tube area of the spilled flow to the inlet capture area, and $D_{spill}/q_l A_{xs}$ is the drag coefficient of this spilled flow, based on its stream tube area ahead of the center-body shock and on the corresponding dynamic pressure q_l. For low-angle center bodies $\left(5^o \text{ wedge or } 12\frac{1^o}{2} \text{ half-angle cone}\right)$, the drag coefficient of this spilled flow is seen to be

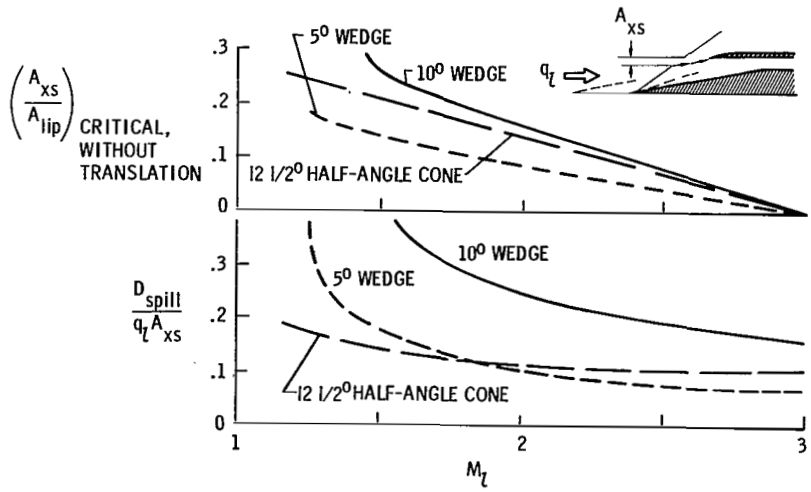

Figure 26.- Drag of inlet spillage flow.

small for flight Mach numbers down to 1.5 where 15 to 25 percent of the flow is bypassed around the inlet.

The amount of inlet spillage can be varied for inlet-engine matching purposes within certain limits by translating or changing the contours of the center body. (Compare results in fig. 26 for 5° and 10° wedge angles.) Attempts to increase the spillage flow an excessive amount, however, cause a breakdown of the supersonic entrance flow and thereby result in greatly increased spillage drag. Cowl lip suction effects compensate for only a small amount of this increased drag, except possibly at transonic Mach numbers. (See refs. 3, 8, 9, and 11.)

Use of an overboard bypass has been found necessary in nearly all high-Mach-number installations for inlet-engine airflow matching and inlet airflow control. Figure 27 presents calculations of the momentum-plus-exit drag of the bypass flow of a typical installation based in part on information and data presented in references 32 to 35. The form of the drag coefficient plotted is identical to that used for the inlet-spillage-drag plot in figure 26, so that a direct comparison can be made.

It is shown in figure 27 that a complete-expansion bypass nozzle with axial discharge provides low drag throughout the entire Mach number range studied. The drawbacks of this type of bypass are the complexity of the nozzle variable geometry and control requirements and the base or boattail drag that exists in cruise if the bypass flow is shut off or reduced a large amount below the design value. The axial sonic nozzle likewise can provide good performance up to Mach numbers of about 2, but is significantly less efficient than the axial complete-expansion nozzle at higher speeds and is subject to the same cruise drag problem. When a "practical" flap nozzle of the type illustrated in

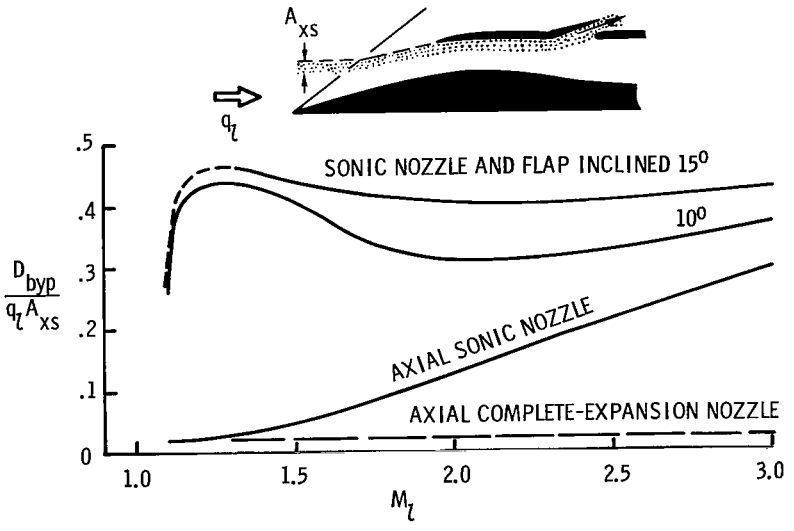

Figure 27.- Drag of overboard bypass flow.

figure 27 is used, the drag is seen to be significantly higher than that associated with critical spillage flow by the inlet. (Compare results in figs. 26 and 27.) Hence, except possibly at transonic speeds, it usually is advantageous to maximize inlet critical spillage flow and to restrict the overboard bypass flow to the minimum required for inlet control purposes or off-design operational requirements such as are occasioned by variations in atmospheric temperature, and so forth. The drag of the bypass flow is sufficiently high to warrant consideration of incorporation of special design features, such as rpm trim or high and low flowing, in the engine itself to minimize the amount of flow bypassed. More comprehensive design information on efficient overboard bypass arrangements would facilitate optimization of secondary-flow systems, which require very careful handling to avoid excessive installation drag.

As an alternate to the overboard bypass, air taken in by the inlet in excess of the engine requirement can be bypassed to the ejector so long as its pressure is high enough to satisfy ejector pumping requirements. (See refs. 36 and 37.) As shown in figure 19, bypass valves usually are incorporated in the ducting to prevent reverse flow at some low-Mach-number operating conditions and to throttle the bypass flow to the desired value when excess upstream pressure is available.

The optimum amount of bypass flow to the ejector is established by engine cooling requirements, the ejector nozzle selected, and the performance trade with overboard bypass. The characteristics of the nozzle selected tend to play a dominant role in the design trade-off. If a simplified nozzle – for example, a fixed shroud design (refs. 28 and 38) or a design incorporating shroud throat area variation only (refs. 26 and 28) – is used, moderate or large amounts of secondary flow may yield large performance improvements over a wide range of operating conditions. These improvements result from beneficial aerodynamic effects on the expansion process of the primary flow. At the other extreme, little if any performance gain would be expected for a highly sophisticated nozzle designed to provide essentially full expansion of the jet flow under all important operating conditions. Most practical nozzles fall between these two extremes.

The effect of secondary flow on the performance of a continuously variable ejector nozzle is difficult to determine accurately because of the large number of geometric variables which must be optimized and because the differences studied are small compared with the total gross thrust. Nevertheless, inasmuch as the designer faces the problem of determining the effect of secondary flow, an attempt has been made to calculate this effect.

A study was conducted first to establish a realistic base-line variable-flap ejector for a Mach 3 afterburning turbojet operating over a typical supersonic transport mission profile. Restraints imposed were limitation of the design secondary flow to the minimum amount required for cooling, limitation of the flap lengths to values determined to be

acceptable from the weights viewpoint in other studies, and limitation of the maximum nozzle-exit diameter to a value equal to the nacelle diameter. Inasmuch as the overall drag of a properly designed installation has been shown to be relatively insensitive to nacelle size, the basic nacelle diameter chosen was large enough to pass up to 30 percent of the secondary flow around the engine without difficulty. The data of reference 27 then were corrected for temperature and real-gas effects and were used to estimate the effects on performance of increasing the secondary flow.

Results of the ejector secondary-flow calculations are presented in figure 28 in terms of a force coefficient which sums the effect of the secondary flow on nozzle gross thrust with the ram drag of this flow. This force coefficient is directly comparable to the drag coefficients given in figures 26 and 27 and is plotted with thrust values (negative drag values) below the axis to maintain parallelism of figure format. Maximum attainable values of the secondary-to-primary flow ratio $\left(\frac{w_{sec}}{w_p}\right)_{max}$, as established by the estimated secondary-flow pressure and the ejector pumping characteristics, are spotted along the curves.

For the maximum-dry-thrust operating condition, which is of critical importance in the supersonic cruise part of the mission, there is little or no drag penalty involved in increasing the amount of secondary flow handled by the ejector up to secondary-to-primary flow ratios as high as 30 percent. At the same time, however, little performance improvement is possible through increasing this flow because both the inlet spillage flow and the overboard bypass flow are negligible at the cruise Mach number (see fig. 25) unless nonstandard operating conditions are encountered.

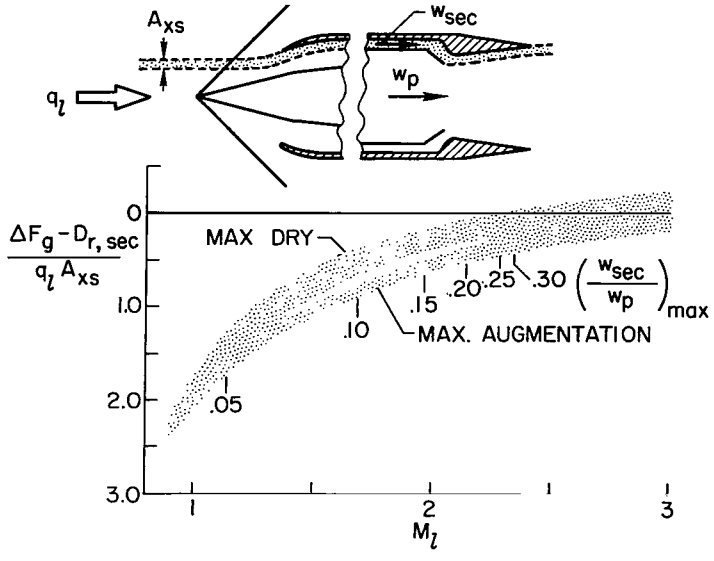

Figure 28.- Drag of bypass flow to continuously variable turbojet ejector nozzle.

For the maximum-augmentation operating condition, which applies to the climb and acceleration phases of the assumed supersonic transport mission, increases in the amount of secondary flow to the ejector in excess of the minimum cooling requirement of about 4 percent is strongly beneficial. It both increases the net thrust and reduces the amount of flow which must be disposed of by inlet spillage or overboard bypass. Thus, in this particular operating condition, bypassing excess inlet capture flow to the ejector provides

higher installation efficiency than can be obtained by either increasing the inlet critical flow spillage or increasing the amount of overboard bypass flow. It is unfortunate that the pumping characteristics of this and other typical ejectors prevent the handling of more than about 5 to 10 percent of the basic engine flow in the range of Mach numbers from 1 to 1.5 where excess flow handling requirements are a maximum. As a result even when both inlet critical flow spillage and the bypass flow to the ejector are maximized, large amounts of excess flow still must be disposed of by overboard bypass, the least efficient method. (See fig. 25.)

A breakdown of the secondary-flow drag of a typical propulsion system designed for a supersonic transport is presented in figure 29. The drag increments shown correspond to the airflow breakdown presented as figure 25 and have been carefully optimized on the basis of the considerations outlined in the preceding discussion. It is indicated that, even when optimized, the secondary-flow-system drag (difference between boundary curves above and below axis) constitutes a signficant fraction of the airplane total drag at transonic and low supersonic speeds for which the airplane thrust-minus-drag margin is a minimum. This fact emphasizes the need for conducting a careful analysis of the secondary-flow drag problem of each new engine installation.

The net secondary-flow-system drag is indicated in figure 29 to be slightly negative in the vicinity of $M = 2.2$ because of the highly favorable effects of secondary flow on ejector performance. This result is subject to question, with the most probable source of error being the accuracy of the basic ejector data used in the calculations. These were the best data available. It is obvious that more experimental work is needed to provide a

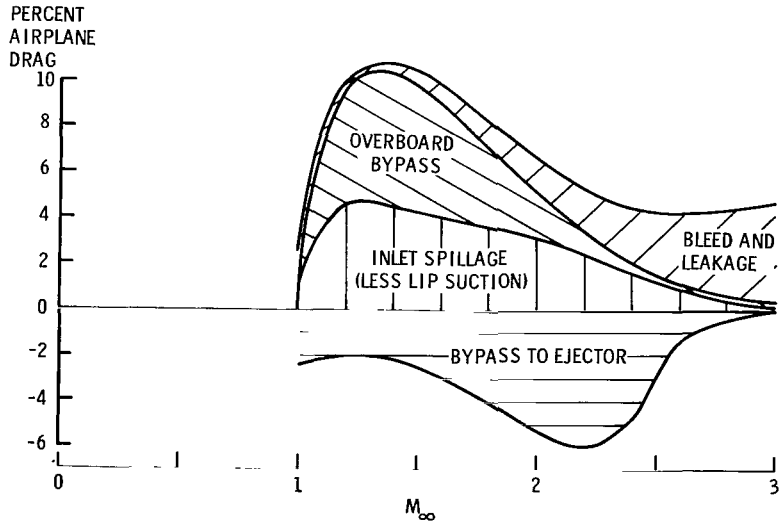

Figure 29.- Breakdown of secondary-flow drag of a typical propulsion system.

range of reliable large-scale hot-flow ejector data for the use of the propulsion-system designer in making meaningful and accurate trade-off studies.

Afterbody drag.- The new aerodynamic tools discussed in a previous section obviously are applicable to the design of the airplane afterbody. However, this part of the airplane operates in a boundary-layer and flow-field environment established by the airplane forebody. In addition, it is subject to important airplane arrangement and balance constraints which tend to require the use of low fineness ratios and, occasionally, steep boattails and blunt bases. As a result, the drag of the afterbody tends to be disproportionately high. Figure 30 shows a photograph of a carefully designed twin-engine fighter research model investigated in the Langley 16-foot transonic tunnel. Hydrogen-peroxide rocket motors were used to provide jet simulation. The model was broken at the parting line, with the external surfaces aft of this line including the nacelle afterbodies and the tails supported on a separate balance. The afterbody drag – that is, the pressure and viscous drag of all external airplane surfaces aft of the model parting line – amounted to 40 to 45 percent of the overall model drag, although the afterbody portion of the model comprised only one-third of the model length and had only one-third of the total wetted area. In less carefully optimized configurations, the drag of this part of the airplane has been found to be even higher – as much as 55 percent of the total. Thus, it is clear that the shaping of components and the handling of the associated aerodynamic interferences for the afterbody are of even more critical importance than for the airplane forebody.

An investigation of the boattail-drag characteristics of a single-engine fighter model (ref. 39) affords a quantitative feeling for the importance of afterbody interference effects for this familiar airplane configuration. Again, the model incorporated a hydrogen-peroxide rocket motor for simulation of the airplane hot jet exhaust flow. As shown in figure 31, the afterbody surface shape was an irregular truncated cone with the vertical and horizontal tails attached directly thereto. Several boattail angles were investigated. The pressure drag of the boattail surface was determined for each case by integration of surface pressure measurements. A comparison, for a typical cruise operating condition, of the results of the experimental measurements with estimates

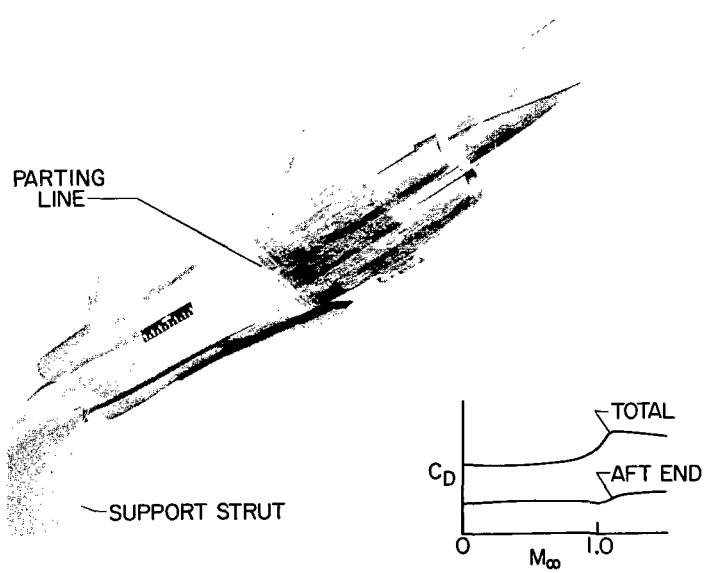

L-2614-1
Figure 30.- Afterbody drag of fighter model.

made for equivalent conical afterbodies by utilizing the experimental data of references 40 to 42 as a basis shows that the interference drag was several times as large as the basic boattail drag predicted without forebody and tail interference effects considered. The pressure drag of the tail surfaces likewise would be increased by the same interference flows. For this airplane, the boattail drag was reduced to an acceptable level by increasing the afterbody fineness ratio (i.e., reducing the average boattail angle from 15^{o} to 6^{o}). Additional reductions could be made, if required, by thinning and staggering the tail surfaces.

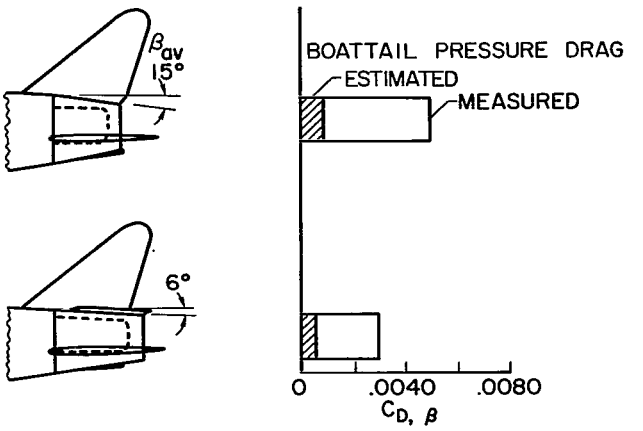

Figure 31.- Afterbody interference drag in cruise for a single-engine fighter model. $M_{\infty} = 0.90$; $\alpha = 0^{o}$; $p_{t,j}/p_{\infty} = 3$; $\frac{A_{\beta,proj}}{S} = 0.092$.

The pressure drag of an isolated nacelle boattail can be calculated for the supersonic speeds by linear theory (e.g., see refs. 21, 43, and 44) or characteristics theory. A wide range of experimental data also exists (e.g., see refs. 21 and 45). Nacelle afterbody shapes investigated in connection with the previously discussed study of the excess-flow optimization problem for the nacelle of a supersonic transport are shown in the top part of figure 32. The primary design trades considered were the amount of internal nozzle expansion provided and the external flap length. It is noted that the boattail angle

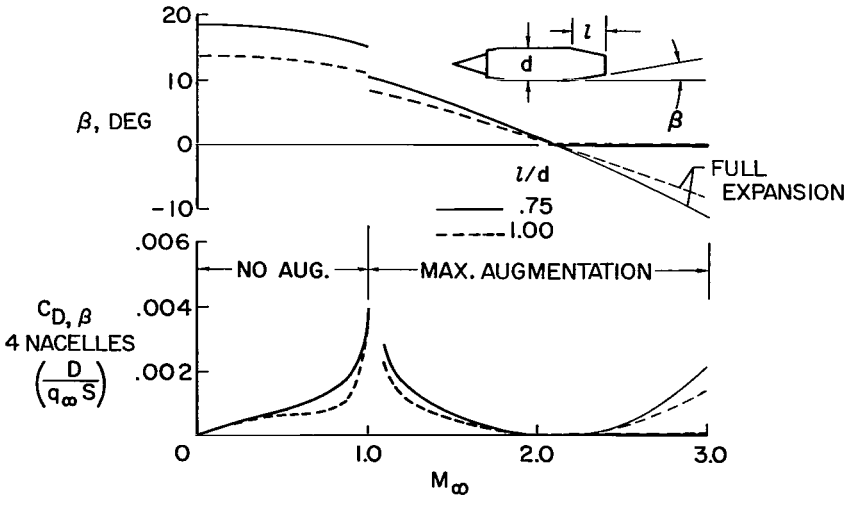

Figure 32.- Boattail drag for nacelle with typical ejector nozzle. $\frac{A_{4N}}{S} = 0.017$.

was held at 0° for Mach numbers between 2 and 3 rather than introducing the outward flare required to permit full expansion of the jet flow (light extensions of curves). The reason for this choice was that the flare drag penalty (see lower part of figure) was found to be approximately an even trade-off with the gain in internal thrust obtained by incorporating the flare; also the low augmentation cruise nozzle setting did not require such a flare to provide essentially full expansion of the jet flow. The longer flap length ($l/d = 1.00$) is shown by the drag calculations to provide somewhat lower drag than the shorter flap length ($l/d = 0.75$) in the high subsonic and transonic speed ranges. Available flap weight data indicated, however, that this reduction in drag was counterbalanced for the supersonic transport mission considered by the associated increased weight. Therefore, the shorter flap length was used for this application. A similar trade-off study must be made for each new installation. When strong flow interferences exist in the region of the nacelle boattail or when subsonic cruise performance is more important, the longer boattail flap is likely to be preferred.

Base drag.- Fixed external afterbody surfaces are used in many airplanes because of weight and complexity considerations. The XB-70A (fig. 33) affords an example of this design approach for a multiengine pack-type propulsion installation. It is noted that the afterbody of this airplane incorporates only a moderate amount of boattailing so that large base areas exist around the nozzle shrouds for all operating conditions. Although definitive base-drag data are not yet available for the airplane itself, pressure measurements obtained for a clustered-exit research model (see lower part of fig. 33 and refs. 46 and 47) indicate that the drag associated with the base areas of the engine pack will be significant at transonic and low supersonic Mach numbers. The XB-70A feature of disposing of available low-energy airflows through the base areas is shown in numerous investigations (e.g., refs. 48 to 51) to provide a reduction in base drag. The dashed curve is an estimate, based on these references, of the base pressure for a bleed flow equal to 3 percent of the primary engine airflow. It is emphasized that the drag reduction corresponding to the increase in base pressure shown, while significant, depends on the availability of large quantities of energy-depleted air; also the drag reduction attainable with base

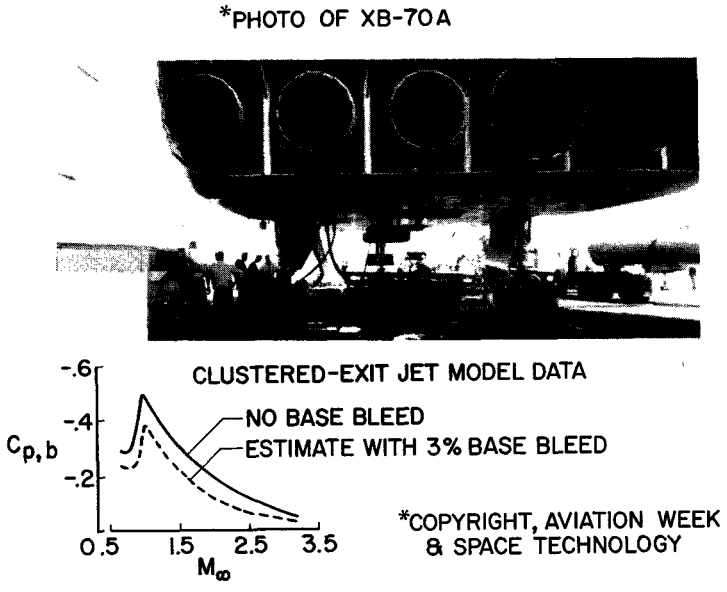

L-2614-28

Figure 33.- Base drag for a multiengine pack-type propulsion installation.

bleed generally is much lower than that attainable with efficient boattailing. It should be noted that this off-design drag problem is not of crucial importance for the XB-70A which is optimized for cruise at $M \approx 3$ and is not forced by sonic-boom considerations to perform its transonic acceleration at high altitudes. However, an off-design drag increment of the magnitude indicated certainly would not be tolerable for a supersonic transport for which the sonic boom is a critical design factor.

The twin-engine fighter model discussed previously in connection with figures 8 and 9 provides a second example of base-drag problems occasioned by the use of fixed-geometry afterbody surfaces. In subsonic cruise operation the primary nozzles of this particular airplane are closed to the nonafterburning position, with annular bases being formed between the nozzles and the nacelle afterbody surfaces. In addition, airplane base areas exist between the nacelles and the fuselage. (See fig. 34.) Model test results from reference 18 presented in figure 34 indicate that the increment in drag coefficient associated with these base areas ranges from about 25 to 50 airplane drag counts. This level of base drag is sufficient to limit seriously the range and endurance capability of the airplane. Obviously, incorporation of a variable-geometry nacelle afterbody surface in the design is one way of minimizing the performance penalty. Results presented in reference 18 show that the base-drag penalty for this type of engine installation also can be reduced by modifying the fuselage shape in accordance with area-rule principles to increase the static pressures and reduce interference flow velocities in the vicinity of the jet exits.

The base-drag characteristics of blunt-based single-engine pods were studied in the course of a transonic wind-tunnel investigation of a four-nacelle research model. Results obtained for an angle of attack of 0° are presented as figure 35. At high subsonic speeds, the base drag of the two inboard nacelles was found to be more than twice that of the two outboard nacelles. This dramatic difference is traceable directly to the zero-lift area distribution of the model which resulted in the formation of a region of low pressure in the vicinity of the inboard nacelle bases. A boattailed nacelle would be expected to experience similar drag penalties. Thus, the inboard nacelle location studied would be ruled out

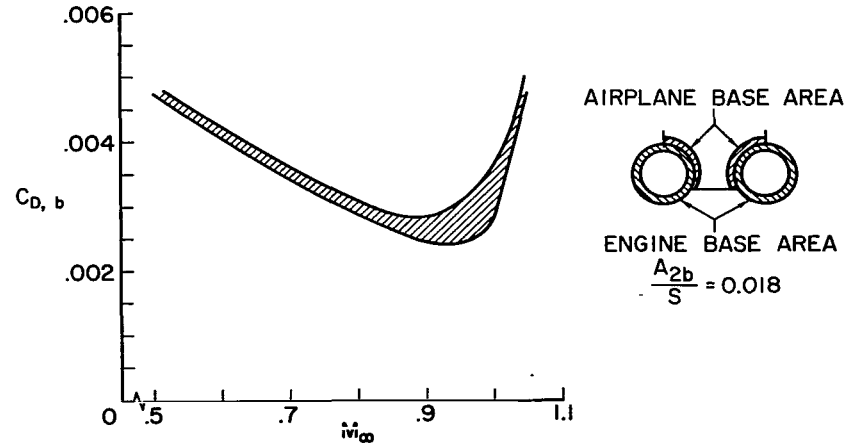

Figure 34.- Base drag for a twin-engine fighter model with overhanging tail boom.

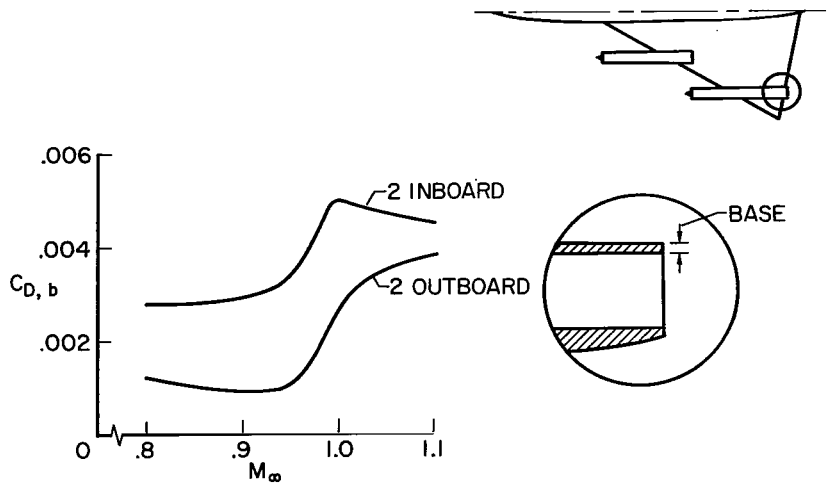

Figure 35.- Base drag of blunt-based single-engine pods. $\alpha = 0^o$; $\frac{A_{2b}}{S} = 0.0073$.

for many present-day applications wherein flight efficiency in low-level dash operation is a primary consideration.

As would be inferred from the previous discussion of figures 1 to 3, angle-of-attack effects were found to be favorable on the flow-field environment of the afterbodies of the inboard nacelles. When the model angle of attack was increased to values representative for high-altitude cruise (4^o to 6^o), the excessive base drag of these nacelles essentially was eliminated. In consequence, the inboard nacelle position studied is still competitive with other nacelle positions for airplanes not required to execute protracted sea-level dashes.

The results in figures 30 to 35 stress the fact that the afterbody of the propulsion installation constitutes an important source of aircraft drag. In high-performance aircraft a strong effort must be made to keep the effective afterbody fineness ratio of the installation high, to minimize base areas, and to configure the aircraft so as to avoid adverse interference effects.

CONCLUDING REMARKS

The present survey indicates that the advance of aircraft speeds into the region of Mach numbers from 2.5 to 3 has greatly increased both the difficulty and the importance of the airframe-engine integration process. External aerodynamic interference considerations enter into nearly all phases of the integration problem and have become of almost dominant importance. Recently developed analytical tools permit a rational approach to the treatment of wave-drag interference effects. Other external flow interferences such as shock—boundary-layer interaction effects during inlet unstarts, environmental effects on the performance of ejector nozzles utilizing auxiliary air inlets, and jet effects on aft-located airframe components, are less easily handled. Experimental study is required for each new installation.

From the performance viewpoint the jet nozzle is by far the most critical installation component. All possible avenues for further increasing its efficiency must be explored, including the possibility of exploiting favorable external-internal flow

interference effects. Even with existing concepts, additional experimental work is needed to provide a range of reliable large-scale hot-flow ejector data broad enough to permit the designer to make meaningful and accurate trade-off studies.

Additional research on other installation components also can be of significant benefit. For example, the perfection of a high-performance self-starting inlet would ease greatly the inlet control design problem. More comprehensive design information on efficient overboard bypass exit arrangements likewise would facilitate optimization of the secondary-flow systems. These systems require very careful handling to avoid excessive installation drag.

The flow distortion problem is a subject in its own right that requires careful consideration from both the installation and engine design viewpoints. This problem gets progressively more critical as either flight Mach number or engine performance increases. It is clear that a great deal of research effort will have to be devoted to finding ways of improving the uniformity and steadiness of the flow delivered to the engine and of reducing the sensitivity of the engine to distortion.

Langley Research Center,
National Aeronautics and Space Administration,
Langley Station, Hampton, Va., June 24, 1966.

REFERENCES

1. Hasel, Lowell E.; and Kouyoumjian, Walter L.: Investigation of Static Pressures and Boundary-Layer Characteristics on the Forward Parts of Nine Fuselages of Various Cross-Sectional Shapes at $M_\infty = 2.01$. NACA RM L56I13, 1957.

2. Liepmann, H. W.; and Roshko, A.: Elements of Gasdynamics. John Wiley & Sons, Inc., c.1957.

3. Davis, Wallace F.; and Scherrer, Richard: Aerodynamic Principles for the Design of Jet-Engine Induction Systems. NACA RM A55F16, 1956.

4. Swan, Walter C.: A Discussion of Selected Aerodynamic Problems on Integration of Propulsion Systems With Airframe on Transport Aircraft. Aerodynamics of Power Plant Installation, Part 1, AGARDograph 103, Oct. 1965, pp. 23-68.

5. Reinhart, W. A.; and Tjonneland, E.: Inlet Flow Field Studies for the Supersonic Transport. [Preprint] 650198, Soc. Automotive Engrs., Apr. 1965.

6. Gaudet, L.; and Winter, K. G.: Preliminary Measurements of the Flow Field on the Leeside of a Delta Wing of Unit Aspect Ratio at a Mach Number of 2.6 and an Incidence of 15°. Tech. Note No. Aero.2787, Brit. R.A.E., Sept. 1961.

7. Stitt, Leonard E.; and Salmi, Reino J.: Performance of a Mach 3.0 External-Internal-Compression Axisymmetric Inlet at Mach Numbers From 2.0 to 3.5. NASA TM X-145, 1960.

8. Faro, Ione D. V.: Supersonic Inlets. AGARDograph 102, May 1965.

9. Mossman, Emmet A.; Pfyl, Frank A.; and Lazzeroni, Frank A.: Fuselage Side Inlets – A Study of Some Factors Affecting Their Performance and a Comparison With Nose Inlets. NACA RM A55F29, 1956.

10. Samanich, N. E.; Barnett, D. O.; and Salmi, R. J.: Effect of External Boundary Layer on Performance of Axisymmetric Inlet at Mach Numbers of 3.0 and 2.5. NASA TM X-49, 1959.

11. Fabri, J., ed.: Air Intake Problems in Supersonic Propulsion. AGARDograph No. 27, Pergamon Press, 1958.

12. Erdos, John; and Pallone, Adrian: Shock-Boundary Layer Interaction and Flow Separation. RAD-TR-61-23, Res. and Advanced Develop. Div., AVCO Corp., Aug. 15, 1961.

13. Motycka, D. L.; and Murphy, J. B.: Intel-to-Inlet Shock Interference Tests. NASA CR-264, 1965.

14. Moeckel, W. E.: Approximate Method for Predicting Form and Location of Detached Shock Waves Ahead of Plane or Axially Symmetric Bodies. NACA TN 1921, 1949.

15. Moseley, George W.; Peterson, John B., Jr.; and Braslow, Albert L.: An Investigation of Splitter Plates for the Aerodynamic Separation of Twin Inlets at Mach 2.5. NASA TN D-3385, 1966.

16. Love, Eugene S.; Grigsby, Carl E.; Lee, Louise P.; and Woodling, Mildred J.: Experimental and Theoretical Studies of Axisymmetric Free Jets. NASA TR R-6, 1959. (Supersedes NACA RM L54L31 by Love and Grigsby, RM L55J14 by Love, RM L56G18 by Love, Woodling, and Lee, and TN 4195 by Love and Lee.)

17. Küchemann, Dietrich; and Weber, Johanna: Aerodynamics of Propulsion. McGraw-Hill Book Co., Inc., 1953.

18. Foss, Willard E., Jr.; Runckel, Jack F.; and Lee, Edwin E., Jr.: Effects of Boattail Area Contouring and Simulated Turbojet Exhaust on the Loading and Fuselage-Tail Component Drag of a Twin-Engine Fighter-Type Airplane Model. NACA RM L58C04, 1958.

19. Swihart, John M.; and Crabill, Norman L.: Steady Loads Due to Jet Interference on Wings, Tails, and Fuselages at Transonic Speeds. NACA RM L57D24b, 1957.

20. Lee, Edwin E., Jr.; and Swihart, John M.: Tabulated Pressure Data for a 60° Delta-Wing—Body—Tail Model With a Hot Jet Exhausting From a Pylon-Mounted Nacelle. NACA RM L57J22, 1958.

21. Harris, Roy V., Jr.: An Analysis and Correlation of Aircraft Wave Drag. NASA TM X-947, 1964.

22. Carlson, Harry W.; and Middleton, Wilbur D.: A Numerical Method for the Design of Camber Surfaces of Supersonic Wings With Arbitrary Planforms. NASA TN D-2341, 1964.

23. Middleton, Wilbur D.; and Carlson, Harry W.: Numerical Method of Estimating and Optimizing Supersonic Aerodynamic Characteristics of Arbitrary Planform Wings. J. Aircraft, vol. 2, no. 4, July-Aug. 1965, pp. 261-265.

24. Robins, A. Warner; Morris, Odell A.; and Harris, Roy V., Jr.: Recent Research Results in the Aerodynamics of Supersonic Vehicles. Paper No. 65-717, Am. Inst. Aeron. Astronaut., Nov., 1965.

25. Landrum, Emma Jean: Effect of Nacelle Orientation on the Aerodynamic Characteristics of an Arrow Wing-Body Configuration at Mach Number 2.03. NASA TN D-3284, 1966.

26. Greathouse, William K.; and Beale, William T.: Performance Characteristics of Several Divergent-Shroud Aircraft Ejectors. NACA RM E55G21a, 1955.

27. Stofan, Andrew J.; and Mihaloew, James R.: Performance of a Variable Divergent-Shroud Ejector Nozzle Designed for Flight Mach Numbers up to 3.0. NASA TM X-255, 1961.

28. Beheim, Milton A.: Off-Design Performance of Divergent Ejectors. NACA RM E58G10a, 1958.

29. Swihart, John M.; Norton, Harry T., Jr.; and Schmeer, James W.: Effect of Several Afterbody Modifications Including Terminal Fairings on the Drag of a Single-Engine Fighter Model with Hot-Jet Exhaust. NASA MEMO 10-29-58L, 1958.

30. Wyatt, DeMarquis D.: An Analysis of Turbojet-Engine-Inlet Matching. NACA TN 3012, 1953.

31. Sibulkin, Merwin: Theoretical and Experimental Investigation of Additive Drag. NACA Rept. 1187, 1954. (Supersedes NACA RM E51B13.)

32. Hearth, Donald P.; and Connors, James F.: A Performance Analysis of Methods for Handling Excess Inlet Flow at Supersonic Speeds. NACA TN 4270, 1958.

33. Yeager, Richard A.; and Gertsma, Laurence W.: Performance of Several Inlet-Bypass Systems for Matching a Two-Dimensional Variable-Geometry Mach 3.0 Inlet at Mach 1.5 and 2.0. NASA MEMO 2-6-59E, 1959.

34. Vick, Allen R.: An Investigation to Determine the Discharge and Thrust Characteristics of Auxiliary-Air Outlets for a Stream Mach Number of 3.25. NASA TN D-1478, 1962.

35. Connors, James F.; and Wise, George A.: Performance of a Translating-Double-Cone Axisymmetric Inlet With Cowl Bypass at Mach Numbers From 2.0 to 3.5. NACA RM E57H07b, 1957.

36. Hearth, Donald P.; Englert, Gerald W.; and Kowalski, Kenneth L.: Matching of Auxiliary Inlets to Secondary-Air Requirements of Aircraft Ejector Exhaust Nozzles. NACA RM E55D21, 1955.

37. Hearth, Donald P.: Use of Main-Inlet Bypass to Supply Ejector Exhaust Nozzle at Supersonic Speeds. NACA RM E56K08, 1957.

38. Hardy, Jean-Marie; and Delery, Jean: Possibilites Actuelles d'Etude Theorique d'Une Tuyere Supersonique a Double-Flux. Aerodynamics of Power Plant Installation, Part 2, AGARDograph 103, Oct. 1965, pp. 445-478.

39. Norton, Harry T., Jr.; and Swihart, John M.: Effect of a Hot-Jet Exhaust on Pressure Distributions and External Drag of Several Afterbodies on a Single-Engine Airplane Model at Transonic Speeds. NACA RM L57J04, 1958.

40. Henry, Beverly Z., Jr.; and Cahn, Maurice S.: Preliminary Results of an Investigation at Transonic Speeds To Determine the Effects of a Heated Propulsive Jet on the Drag Characteristics of a Related Series of Afterbodies. NACA RM L55A24a, 1955.

41. Cubbage, James M., Jr.: Jet Effects on the Drag of Conical Afterbodies for Mach Numbers of 0.6 to 1.28. NACA RM L57B21, 1957.

42. Silhan, Frank V.; and Cubbage, James M., Jr.: Drag of Conical and Circular-Arc Boattail Afterbodies at Mach Numbers From 0.6 to 1.3. NACA RM L56K22, 1957.

43. Jack, John R.: Theoretical Pressure Distributions and Wave Drags for Conical Boattails. NACA TN 2972, 1953.

44. Fraenkel, L. E.: Curves for Estimating the Wave Drag of Some Bodies of Revolution, Based on Exact and Approximate Theories. C.P. No. 136, British A.R.C., 1953.

45. Cortright, Edgar M., Jr.; and Kochendorfer, Fred D.: Jet Effects on Flow Over Afterbodies in Supersonic Stream. NACA RM E53H25, 1953.

46. Swihart, John M.; and Nelson, William J.: Performance of Multiple Jet-Exit Installations. NACA RM L58E01, 1958.

47. Norton, Harry T., Jr.; Foss, Willard E., Jr.; and Swihart, John M.: An Investigation of Modified Clustered Jet-Exit Arrangements at Supersonic Speeds. NASA TM X-540, 1961.

48. Norton, Harry T., Jr.; and Keith, Arvid L., Jr.: Effect of Base Bleed and Terminal Fairings on the Performance of Exhaust-Nozzle—Afterbody Combinations at Mach Numbers of 1.93, 2.55, and 3.05. NASA TN D-539, 1960.

49. Cubbage, James M., Jr.: Jet Effects on Base and Afterbody Pressures of a Cylindrical Afterbody at Transonic Speeds. NACA RM L56C21, 1956.

50. Beheim, Milton A.; Klann, John L.; and Yeager, Richard A.: Jet Effects on Annular Base Pressure and Temperature in a Supersonic Stream. NASA TR R-125, 1962.

51. Beheim, Milton A.: Flow in the Base Region of Axisymmetric and Two-Dimensional Configurations. NASA TR R-77, 1960.

NASA-Langley, 1966 L-5009

"The aeronautical and space activities of the United States shall be conducted so as to contribute . . . to the expansion of human knowledge of phenomena in the atmosphere and space. The Administration shall provide for the widest practicable and appropriate dissemination of information concerning its activities and the results thereof."

—NATIONAL AERONAUTICS AND SPACE ACT OF 1958

NASA SCIENTIFIC AND TECHNICAL PUBLICATIONS

TECHNICAL REPORTS: Scientific and technical information considered important, complete, and a lasting contribution to existing knowledge.

TECHNICAL NOTES: Information less broad in scope but nevertheless of importance as a contribution to existing knowledge.

TECHNICAL MEMORANDUMS: Information receiving limited distribution because of preliminary data, security classification, or other reasons.

CONTRACTOR REPORTS: Technical information generated in connection with a NASA contract or grant and released under NASA auspices.

TECHNICAL TRANSLATIONS: Information published in a foreign language considered to merit NASA distribution in English.

TECHNICAL REPRINTS: Information derived from NASA activities and initially published in the form of journal articles.

SPECIAL PUBLICATIONS: Information derived from or of value to NASA activities but not necessarily reporting the results of individual NASA-programmed scientific efforts. Publications include conference proceedings, monographs, data compilations, handbooks, sourcebooks, and special bibliographies.

Details on the availability of these publications may be obtained from:

SCIENTIFIC AND TECHNICAL INFORMATION DIVISION

NATIONAL AERONAUTICS AND SPACE ADMINISTRATION

Washington, D.C. 20546